

Article

Coexistence of Thread and Sheet Chaotic Attractors for Three-Dimensional Lozi Map

René Lozi 

LJAD, CNRS, Université Côte d'Azur, F-06000 Nice, France; Rene.LOZI@univ-cotedazur.fr

Abstract: Since its original publication in 1978, Lozi's chaotic map has been thoroughly explored and continues to be. Hundreds of publications have analyzed its particular structure or applied its properties in many fields (electronic devices such as memristors, A.I. with swarm intelligence, etc.). Several generalizations have been proposed, transforming the initial two-dimensional map into a multidimensional one. However, they do not respect the original constraint that allows this map to be one of the few strictly hyperbolic: a constant Jacobian. In this paper, we introduce a three-dimensional piece-wise linear extension respecting this constraint and we explore a special property never highlighted for chaotic mappings: the coexistence of *thread* chaotic attractors (i.e., attractors that are formed by a collection of lines) and *sheet* chaotic attractors (i.e., attractors that are formed by a collection of planes). This new three-dimensional mapping can generate a large variety of chaotic and hyperchaotic attractors. We give five examples of such behavior in this article. In the first three examples, there is the coexistence of *thread* and *sheet* chaotic attractors. However, their shapes are different and they are constituted by a different number of pieces. In the last two examples, the blow up of the attractors with respect to parameter a and b is highlighted.

Keywords: Lozi map; strange attractors; sheet hyperchaotic attractors; thread chaotic attractors; blow up of attractor



Citation: Lozi, R. Coexistence of Thread and Sheet Chaotic Attractors for Three-Dimensional Lozi Map. *Dynamics* **2023**, *3*, 315–344. <https://doi.org/10.3390/dynamics3020019>

Academic Editor: Christos Volos

Received: 5 May 2023

Revised: 31 May 2023

Accepted: 3 June 2023

Published: 9 June 2023



Copyright: © 2023 by the author. Licensee MDPI, Basel, Switzerland. This article is an open access article distributed under the terms and conditions of the Creative Commons Attribution (CC BY) license (<https://creativecommons.org/licenses/by/4.0/>).

1. Introduction

Since its original publication in 1978, Lozi's chaotic map has been thoroughly explored and continues to be. Hundreds of publications have analyzed its particular structure or applied its properties in many fields (cryptography, optimization, secure communications, electronic devices such as memristors, A.I. with swarm intelligence, etc.). Several kinds of generalization have been proposed, transforming the initial two-dimensional map into a multidimensional one. However, they do not respect the original constraint that allows this map to be one of the few strictly hyperbolic: a constant Jacobian. In this paper, we introduce a three-dimensional piece-wise linear extension respecting this constraint and we explore a special property never highlighted for chaotic mappings: the coexistence of *thread chaotic attractors* (i.e., attractors that are formed by a collection of lines) and *sheet hyperchaotic attractors* (i.e., attractors that are formed by a collection of planes).

In Section 2, we recall the history and initial definition of the Lozi map, its chaotic properties in the dissipative case, and the dynamics features (fixed points, invariant manifolds, basin of attraction, etc.). We also describe the chaotic properties in the conservative case. We conduct a rapid survey of the generalization of such a map: topological generalization (*Lozi-like* map), geometrical generalization (*Lozi-type* map), generalization of the formula in a dimension of three or more, fractal generalization, non-conventional generalization, and networks of Lozi maps with chimera. In Section 3, we recall the definition of two Rössler hyperchaotic attractors for comparison, and we introduce a new generalization for the Lozi map in three dimensions. In Section 4, we give the basic properties of the *thread* and *sheet*-attractors (fixed point, period-two orbit). This new three-dimensional mapping can generate a large variety of chaotic and hyperchaotic attractors. We give five examples of

such behavior in this section. In the first three examples, there is the coexistence of *thread* and *sheet* chaotic attractors. However, their shapes are different and they are constituted by a different number of pieces. In the two last examples, the blow up of the attractors with respect to parameter a and b is highlighted. A brief conclusion is drawn in Section 5.

2. The Lozi Map

2.1. History

I discovered what is now called the *Lozi map* exactly on 15 June 1977 around 11 a.m. during the defense of the Ph.D. thesis of one of my colleague in the department of mathematics of the University of Nice (France) [1] (p. xxv).

As I explained in [2], the week before, I attended the International Conference on Mathematical Problems in Theoretical Physics in Roma. The opening talk was given by David Ruelle on 6 June, who conjectured in his presentation that, for the Hénon attractor, the theoretical entropy should be equal to the characteristic exponent [3]. This is how I discovered the first example of chaotic and strange attractors (see Figure 1). Surprisingly, I had never met Michel Hénon before, who worked a few kilometers apart from the math department of the university at the Nice Observatory.

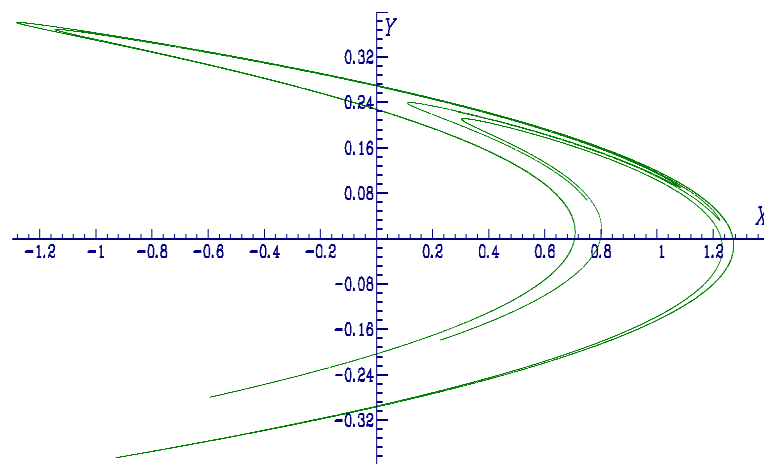


Figure 1. Hénon map (2) for the parameter value $a = 1.4, b = 0.3$, initial value $x_0 = 0, y_0 = 0$.

Hénon, who explored the Lorenz map [4] numerically using an IBM-7040, found it difficult to highlight its inner nature due to its very strong dissipativity. Its rate of volume contraction is given by the Lie derivative of the Lorenz equations, which can be solved. For the parameters chosen by Lorenz, $V(t) = V(0)e^{-\frac{4t}{3}}$. Therefore, after one time unit, volumes are reduced by a factor of 10^6 . Inspired by his astronomer experience of Poincaré’s map for the motion of planets, Hénon built the metaphoric model [5]

$$\begin{cases} x_{n+1} = 1 - ax_n^2 + y_n, \\ y_{n+1} = bx_n, \end{cases} \tag{1}$$

also represented by the iterates of any initial point $(x_0, y_0)^T$ by the map $\mathcal{H}_{a,b} : \mathbb{R}^2 \rightarrow \mathbb{R}^2$

$$\mathcal{H}_{a,b} \begin{pmatrix} x \\ y \end{pmatrix} = \begin{pmatrix} 1 - ax^2 + y, \\ bx. \end{pmatrix} \tag{2}$$

For this map, the contracting properties are only determined by the parameter b . With $b = 0.3$, the contraction in one iteration is mild enough that the sheaves of the attractors are visible. Eventually, he graphically observed the fractal structure of the attractor, which astonished the research community.

2.1.1. Initial Definition

At this time, I was working in numerical analysis, in the domain of bifurcation, which was not very developed in France. My main interest was focused on the discretization problem and finite element method in which nonlinear functions are approximated by piecewise linear ones. During the Roma conference, I tried unsuccessfully to apply the spirit of the method of finite elements to the Hénon attractor. Returning to Nice after this conference, I eventually decided, using paper and pencil, to change the square function of the Hénon attractor, which is U-shaped, into the absolute value function, which has a V shape, implying a folding property (a folding property is important for a horseshoe, a main ingredient of chaos, as highlighted by Stephen Smale [6]).

Right after the defense, I went back to my office and immediately tested this modification in a few minutes on a small desktop computer HP 9820 linked to an HP 9862 plotter. I found a similar attractor of the Hénon attractor, with straight lines instead of curves for the map [7] (see Figure 2).

$$\mathcal{L}_{a,b} \begin{pmatrix} x \\ y \end{pmatrix} = \begin{pmatrix} 1 - a|x| + y, \\ bx. \end{pmatrix} \tag{3}$$

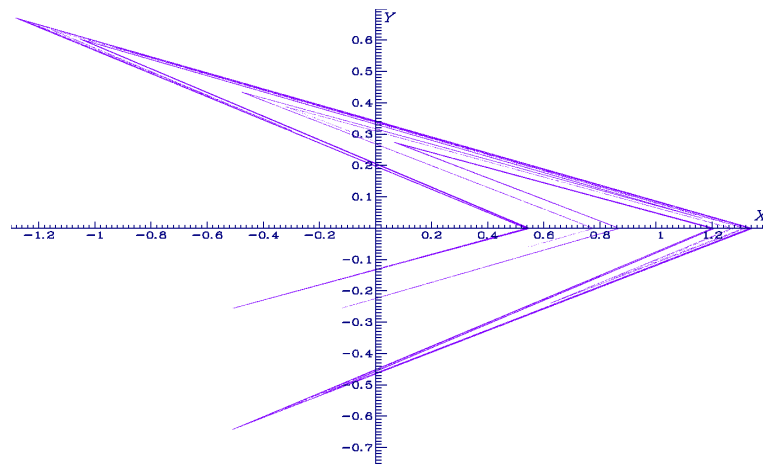


Figure 2. Original Lozi map (3) in dimension 2 for the parameter value $a = 1.7, b = 0.5$, initial value $x_0 = 0, y_0 = 0$.

2.1.2. Chaotic Properties of the Dissipative Map ($|b| < 1$)

When $|b| < 1$, the map is called “dissipative”, which means that the image of any subset Δ by f has a measure that is less than the measure of Δ : $measure(f(\Delta)) < measure(\Delta)$.

Two years after the discovery of this new chaotic attractor and only one year after its publication [7], at the end of 1979, during the *International Conference on Nonlinear Dynamics*, patronized by the New York Academy of Sciences on 17–21 December 1979, Michal Misiurewicz presented a rigorous proof that, for a set of parameters \mathcal{S} , this map has a strange attractor, coining at this occasion the name “Lozi map” [8]. This set in the plane of parameters (a, b) is defined by

$$\mathcal{S} = \left\{ (a, b) \mid b > 0, a\sqrt{2} < b + 2, b < \frac{a^2 - 1}{2a + 1}, 2a + b < 4 \right\}, \tag{4}$$

(see Figure 3).

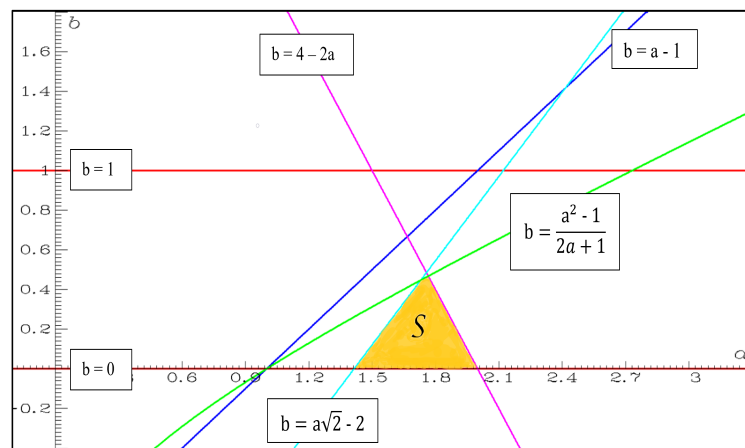


Figure 3. The set S of the plane of parameters where Lozi map has a strange attractor in the first proof of Misiurewicz [8]. Red lines $b = 0$ and $b = 1$, blue line $b = a - 1$, pink line $b = -2a + 4$, cyan line $b = a\sqrt{2} - 2$, green curve $b = \frac{a^2-1}{2a+1}$.

This set of parameters S (defined only for $b > 0$) was later slightly enlarged (as S^+ in Figure 4) in the upper edge of the triangle by Misiurewicz and Stimac [9], removing the condition $b < \frac{a^2-1}{2a+1}$,

$$S^+ = \left\{ (a, b) \mid b > 0, a\sqrt{2} < b + 2, 2a + b < 4 \right\}. \tag{5}$$

Recently, the case $b < 0$ was studied by Kucharski [10], who found a quasi-symmetric set of parameters S^- (Figure 4); however, it is not completely symmetric for the right-hand-side boundary,

$$S^- = \left\{ (a, b) \mid -1 < b < 0, a\sqrt{2} > b + 2, b > \frac{-8a + 3a^2 + \sqrt{-16a^3 + 9a^4}}{8} \right\}. \tag{6}$$

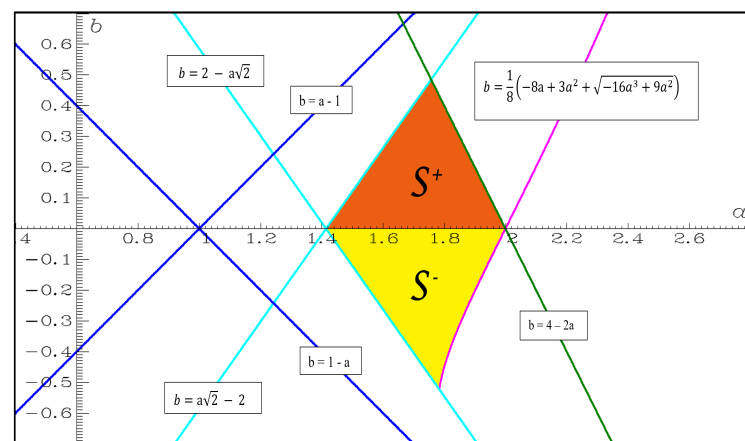


Figure 4. The sets S^+ and S^- of the plane of parameters where Lozi map has a strange attractor in the second proof of Misiurewicz and Stimac [9] and the proof of Kucharski [10]. Blue lines $b = a - 1$ and $b = 1 - a$, cyan lines $b = a\sqrt{2} - 2$ and $b = 2 - a\sqrt{2}$, green line $b = 4 - 2a$, pink line $b = \frac{-8a+3a^2+\sqrt{-16a^3+9a^4}}{8}$.

2.1.3. Fixed Points, Invariant Manifolds and Basin of Attraction

Due to the piecewise linearity of absolute value in $\mathcal{L}_{a,b}$ (3), one can explicitly compute the fixed points and the periodic orbit of any order of it.

When $1 - a < b < a + 1$ (for $a > 0$, both regions S^- and S^+ are in the cone defined by these inequalities), there exist two fixed points

$$\mathcal{A} = \left(\frac{1}{a + 1 - b}, \frac{b}{a + 1 - b} \right),$$

which belongs to the quadrant $\{x \geq 0, y \geq 0\}$, and

$$\mathcal{B} = \left(\frac{1}{1 - a - b}, \frac{b}{1 - a - b} \right),$$

which belongs to the quadrant $\{x < 0, y < 0\}$.

Furthermore, one can easily compute the local stability of these points by evaluating the corresponding eigenvalues of the Jacobian matrix of $\mathcal{L}_{a,b}$ and conclude that, in the domain of the parameter space where both \mathcal{A} and \mathcal{B} coexist—that is, for $a > |b| + 1$ —they are saddle points.

Interestingly, the chaotic attractor of the Lozi map belongs to the unstable invariant manifold of \mathcal{A} . More exactly, from [8], it is known that the chaotic (and strange) attractor $\tilde{\mathcal{F}}$ can be constructed from the successive forward iterations of a trapping region F ,

$$\tilde{\mathcal{F}} = \bigcap_{n=0}^{\infty} \mathcal{L}^n(F),$$

where F is the triangle with vertices at the points I , $\mathcal{L}(I)$, and $\mathcal{L}^2(I)$, and I is the point given by the intersection of the unstable manifold of the fixed point \mathcal{A} with the horizontal axis

$$I = \left(\frac{2 + a + \sqrt{a^2 + 4b}}{2(1 + a - b)}, 0 \right).$$

Baptista et al. [11] found that the basin of attractor is modeled by some parts of the stable manifold of the fixed point \mathcal{B} . They considered the point X intersection of this stable manifold with the vertical axis. A simple computation gives its expression as

$$X = \left(0, \frac{b(2 - a + \sqrt{a^2 + 4b})}{(a - \sqrt{a^2 + 4b})(a + b - 1)} \right),$$

and a certain point T belonging on the horizontal axis, first defined by Ishii [12], whose expression is

$$X = \left(\frac{b(2 - a + \sqrt{a^2 + 4b})(a(1 + b) + (1 - b)\sqrt{a^2 + 4b})}{(1 - a - b)(a - \sqrt{a^2 + 4b})(a - \sqrt{a^2 + 4b})(2b(b - 1) + a^2(1 + 2b) + a(1 - 2b)\sqrt{a^2 + 4b})}, 0 \right).$$

They showed that the basin of attraction is bounded by a polygonal line entirely characterized by the points T and X and their successive preimages.

2.1.4. Other Dynamical Properties of the Dissipative Map ($|b| < 1$)

Boroński, Kucharski, and Ou [13] rigorously determined an open region in the parameter space for which the Lozi map exhibits periodic points of least period n for all $n > 13$:

$$\mathcal{P}_{str} = \{(a, b) \mid b > 0, b < l_{str}(a) \text{ when } a < a_0, \text{ and } b < l_{tan}(a) \text{ when } a > a_0\}, \quad (7)$$

and

$$\mathcal{P}_3(a, b) = \{(a, b) \mid 0 \leq b \leq 1, a > l_{hyp}(b), \text{ and } a > l_3(b)\}, \quad (8)$$

where

$$a_0 = \frac{2}{7}(2 + 3\sqrt{2}) \approx 1.78, \quad l_{str}(a) = -2 + \sqrt{2}a,$$

$$l_{tan}(a) = \frac{1}{8} \left(8a - 3a^2 - \sqrt{9a^4 - 16a^3} \right), l_{hyp}(b) = b + 1,$$

and

$$l_3(b) = \frac{1}{2} \left[1 - b + \sqrt{(1 - b)^2 + 4(1 - b + b^2)} \right].$$

Theorem 1 ([13]). For all $(a, b) \in \mathcal{P}_{str} \cap \mathcal{P}_3$, the Lozi map $\mathcal{L}_{a,b}$ has a periodic point of least period n for $n = 1, 2, 3$ and all $n > 13$.

It is not in the scope of this article to provide a survey of all the papers describing the other dynamical or statistical properties of the Lozi map because they are too numerous. One may refer to [1] for a compendium of results published between 1997 and 2013. Below, only some particular or more recent results are pointed out.

Many authors have published results on bifurcations of such a map, such as Botella-Soler et al. [14] showing that it presents what they call *bisecting bifurcations*: those that are mediated by an infinite set of neutrally stable periodic orbits.

Sushko et al. [15] investigated the bifurcation structure of the parameter plane in the vicinity of the curve related to a center bifurcation of the fixed point. A distinguishing property of the Lozi map is that it is conservative (see Section 2.1.5) at the parameter value corresponding to this bifurcation. As a result, the bifurcation structure close to the center bifurcation curve is quite complicated. In particular, an attracting fixed point (focus) can coexist with various attracting cycles, as well as with chaotic attractors, and the number of coexisting attractors increases as the parameter point approaches the center bifurcation curve. Their study also contributes to the border collision bifurcation theory since the Lozi map is a particular case of the 2D border collision normal form (2D-BCNF).

Glendinning and Simpson [16] used, as a canonical example, the following 2D-BCNF, which is the family of difference equations $(x, y) \rightarrow f(x, y)$:

$$f(x, y) = \begin{cases} A_L \begin{bmatrix} x \\ y \end{bmatrix} + \begin{bmatrix} \mu \\ 0 \end{bmatrix}, & x \leq 0, \\ A_R \begin{bmatrix} x \\ y \end{bmatrix} + \begin{bmatrix} \mu \\ 0 \end{bmatrix}, & x \geq 0, \end{cases} \tag{9}$$

and with

$$A_L = \begin{bmatrix} \tau_L & 1 \\ -\delta_L & 0 \end{bmatrix}, \quad A_R = \begin{bmatrix} \tau_R & 1 \\ -\delta_R & 0 \end{bmatrix}.$$

In their paper, they restricted their attention to the parameter values $\tau_R \in \mathbb{R}$, $\tau_L > 0$, $\delta_L > 0$, $\delta_R > 0$, $\mu = 1$, for which f is invertible and orientation-preserving.

The role of μ is to control the border-collision bifurcation. In view of a linear rescaling, it is only needed to be considered for the values $\{-1, 0, 1\}$ (here, it is 1). The condition $\tau_L > 0$ is needed for the definition of the induced map. If $\tau_L = -\tau_R$ and $\delta_L = \delta_R$, then the 2D BCNF reduces to the Lozi map.

In addition to bifurcation studies, Collet and Levy [17] considered ergodic properties of such mapping, which they consider as an intermediate stage between the axiom A dynamical systems and more complicated systems, such as the Hénon map. They constructed its Bowen–Ruelle measure and also derived some of its properties, which are similar to those of an axiom A system.

Rychlik [18] gave a proof of the existence of Sinai–Bowen–Ruelle measures (SBR measures) for this map. He also proved that the number of SBR measures is finite. Cao and Liu [19] explored the geometric structure of its chaotic attractor and proof:

Proposition 1. *If the parameters (a, b) satisfy Misiurewicz conditions (4), then the strange attractor $\Lambda_{a,b}$ possesses the following properties:*

- *The union of the transversal homoclinic points and weak transversal homoclinic points is dense in $\Lambda_{a,b}$;*
- *All periodic points are hyperbolic;*
- *The set of periodic points forms a dense set in $\Lambda_{a,b}$;*
- *Any two hyperbolic points form a transversal heteroclinic cycle or a weak transversal heteroclinic cycle.*

Other statistical (hyperbolic, ergodic, and topological) properties are described in the study by Afraimovich et al. [20].

The symbolic dynamics of this map have also been greatly studied. In 1991, Zheng [21], described some details of it. Two families of symbolic sequences were assigned for two groups of lines in the phase plane, the order of symbolic sequences was defined, and the ordering rules were derived. Misiurewicz and Stimac [9], in a more detailed study, introduced the set of kneading sequences for this map and proved that it determines its symbolic dynamics. They also introduced two other equivalent approaches. One can also cite in this field of research the important works of Ishii [12,22], Sand [23], and de Carvalho and Hall [24].

In [12], Ishii constructed a kneading theory *à la* Milnor–Thurston and showed that the topological properties of the dynamics of the Lozi map are determined by its pruning front and primary pruned region only. This gives a solution to the first tangency problem for the Lozi family; moreover, the boundary of the set of all horseshoes in the parameter space was shown to be algebraic. As an application of this result, in [22], the partial monotonicity of the topological entropy and of bifurcations near horseshoes was proved. Upper and lower bounds for the Hausdorff dimension of the Lozi attractor were also given in terms of parameters. In [24], recent results on pruning theory were given, concentrated on prunings of the horseshoe. In [23], the monotonicity of the Lozi family when the Jacobian determinant is close to zero was shown. The main ingredients of the proof therein were the “pruning pair method” and a detailed analysis of the parameter dependence of the kneading invariant of the tent-map family.

2.1.5. Chaotic Properties of the Conservative Map ($|b| = 1$)

In the conservative case (also called area preserving) $measure(f(\Delta)) = measure(\Delta)$, there is no attractor.

Li et al. [25] studied this case and highlighted that it can generate initial-values-related coexisting infinite orbits. Its moving orbits are extremely dependent on its initial values and present periodic, quasi-periodic, and chaotic orbits, with different types and topologies. In other words, the emergence of extreme multistability appears in the area-preserving Lozi map. As an example, several of such orbits are plotted in (Figures 5 and 6). Li et al. noted that the coexistence of double or multiple attractors has been found in the Hénon map, the M-dimensional nonlinear hyperchaotic model [26], and the multistage DC/DC switching converter [27], and that two types of simple 2D hyperchaotic maps with sine trigonometric nonlinearity and constant controllers were shown to generate initial-boosted infinite attractors along a phase line [28,29]. Recently, a simple two-dimensional sine map was presented to obtain the initials-boosted infinitely many attractors along a phase plane [30]. However, they emphasized that all these newly presented discrete maps only exhibit the coexisting attractors with different positions. However, the coexisting infinite attractors with different topologies and different positions in the discrete maps are rarely reported like those in the area-preserving Lozi map.

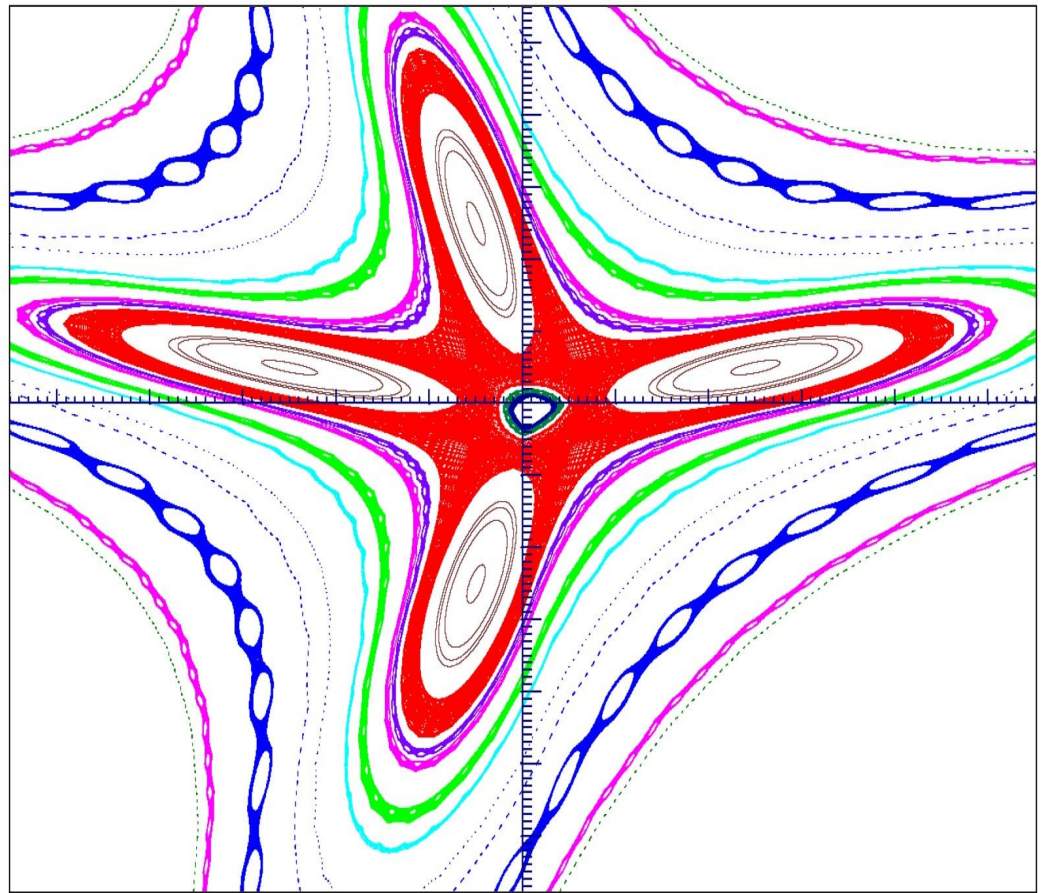


Figure 5. Periodic, quasi-periodic, and chaotic orbits of the area-preserving map (3) in the plane (x, y) when $a = 0.5$ and $b = -1$. Initial values: red (most extended chaotic orbit) $x_0 = 1.3, y_0 = 2.0$, dark blue (innermost chaotic orbit inside the red orbit) $x_0 = 1.3, y_0 = -0.2$, dark green (chaotic orbit inside the red orbit $x_0 = 1.7, y_0 = -0.2$ (see magnified Figure 6)). Initial values of the 4 brown periodic ellipse-shaped orbits belonging to the 4 ellipsoids inside the red region $x_0 = 10.0, y_0 = 2.3, x_0 = 10.0, y_0 = 3.0, x_0 = 10.0, y_0 = 3.2, x_0 = 10.0, y_0 = 3.3$. From origin to upper right corner: purple (chaotic orbit) $x_0 = 10.0, y_0 = 4.6$, magenta (chaotic orbit) $x_0 = 10.0, y_0 = 5.0$, light green (chaotic orbit) $x_0 = 10.0, y_0 = 6.0$, light blue (chaotic orbit) $x_0 = 10.0, y_0 = 6.8$, dark blue (quasiperiodic orbit) $x_0 = 10.0, y_0 = 8.5$, blue (quasiperiodic orbit) $x_0 = 10.0, y_0 = 9.6$, dark blue (chaotic orbit) $x_0 = 10.0, y_0 = 13.0$, pink (chaotic orbit) $x_0 = 10.0, y_0 = 16.0$, green (quasiperiodic orbit) $x_0 = 10.0, y_0 = 17.0$.

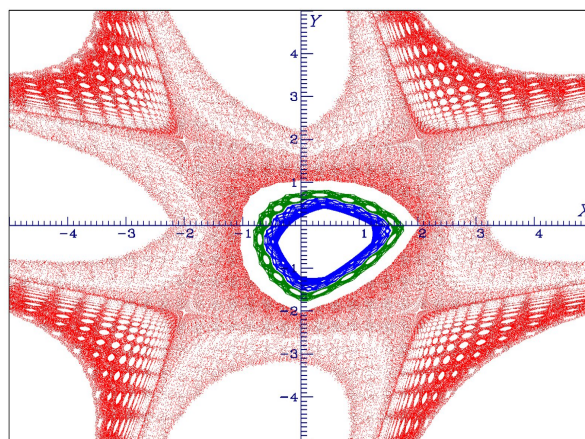


Figure 6. Magnification of the central part of Figure 5.

In addition to the analysis of Sushko et al. [15] (see Section 2.1.4), this conservative map was also studied by Lopesino et al. in [31], who proved, when $a > 4$, the existence of a chaotic saddle in the square

$$S_q = \{(x, y) \in \mathbb{R}^2 \mid |x| \leq R, |y| \leq R\},$$

with

$$R = R(a) = \frac{a}{4(a - 2)}. \tag{10}$$

2.2. Generalizations

A general trend in mathematics is to generalize any new mathematical object. Due to the simplicity of the equations defining the Lozi map (3), the simplest way to generalize it is to increase the dimension of the discrete dynamical system associated by adding similar equations. The same was carried out for the Hénon map (2) (see [32] for a survey). Another way is to generalize its topological or geometrical properties, and a recent third way is to define this map in the new paradigm of fractional mappings. Besides these ways, recently, a non-conventional generalization entangling this map with cosine and exponential functions has been proposed. Additionally, the Lozi map can be used to construct networks of chaotic attractors, either alone or with a Hénon map.

It is the second way that was first explored in 1985 by Lai-Sang Young [33], who defined a *generalized Lozi map* (also called *Lozi-like map*), and later in 2018 by Misiurewicz and Stimac [34], who defined another kind of *Lozi-like map* without any reference or relationship with the definition of Young. Instead, Juang and Chang [35] defined in 2010 a geometrical generalization called a *Lozi-type map*.

2.2.1. Topological Generalizations: Lozi-like Maps

Let $\mathcal{R} = [0, 1] \times [0, 1]$ and let $f : \mathcal{R} \rightarrow \mathcal{R}$ be a continuous injective map. Suppose that f (or some iterate of f) takes \mathcal{R} into its interior.

Definition 1 ([33]). A continuous injective map $f : \mathcal{R} \rightarrow \mathcal{R}$ of $\mathcal{R} = [0, 1] \times [0, 1]$ is a *generalized Lozi map* if it satisfies the following conditions.

- (L.1) There exists $0 < a_1 < \dots < a_n < 1$ such that f is a C^1 -diffeomorphism on $\mathcal{R} \setminus \bigcup_{i=1}^n Y_i$, where $Y_i = \{a_i\} \times [0, 1]$. From now on, we set $\mathcal{S} = \bigcup_{i=1}^n Y_i$.
- (L.2) The norm of the derivative Df of f is uniformly bounded on $\mathcal{R} \setminus \mathcal{S}$, i.e.,

$$M_f = \sup\{\|Df_x\|; x \in \mathcal{R} \setminus \mathcal{S}\} < \infty,$$

where $\|Df_x\| = \sup\{\|Df_x(\mathbf{v})\|\}; \mathbf{v} \in T_x(\mathcal{R}), \|\mathbf{v}\| = 1$.

- (L.3) There exist constants $|\lambda^s| < 1 < |\lambda^u|$ and continuous cone-fields $C^s = \{C_x^s\}_{x \in \mathcal{R}}$, $C^u = \{C_x^u\}_{x \in \mathcal{R}}$ on \mathcal{R} such that, for any $x \in \mathcal{R} \setminus \mathcal{S}$ and any vectors $\mathbf{v} \in C_x^u, \mathbf{w} \in C_{f(x)}^s$,

- $Df_x(C_x^u) \subset C_{f(x)}^u$ and $\|Df_x(\mathbf{v})\| \geq |\lambda^u| \|\mathbf{v}\|$,
- $Df_x(C_{f(x)}^s)^{-1} \subset C_x^s$ and $\|Df_{f(x)}^{-1}(\mathbf{w})\| \geq (|\lambda^s|)^{-1} \|\mathbf{w}\|$.

We say that C^s, C^u are stable and unstable cone-fields of f , respectively.

Figure 7 illustrates the image $f(\mathcal{R})$ of \mathcal{R} using a generalized Lozi map f .

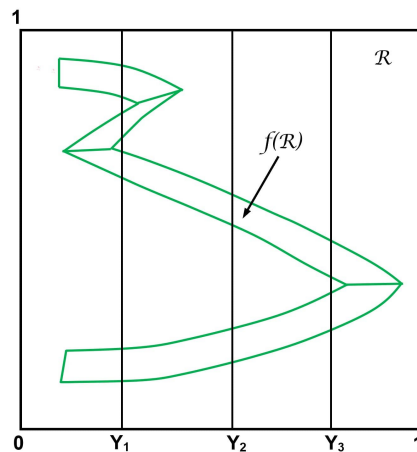


Figure 7. Image $f(\mathcal{R})$ of \mathcal{R} using a generalized Lozi map f in the sense of Young [33].

In [33], Lai-Sang Young proved that *Lozi-like maps* have invariant measures with absolutely continuous conditional measures on unstable manifolds. As a consequence, they have Bowen–Ruelle measures. More recently, Sakurai [36] showed that certain *Lozi-like maps* have an orbit-shifted shadowing property.

Another kind of topological generalization also called a *Lozi-like map*, was recently introduced by Misiurewicz and Stimac [34]. Its definition is not straightforward and needs some preliminaries.

Definition 2 ([34]). Let $F_1, F_2 : \mathbb{R}^2 \rightarrow \mathbb{R}^2$ be C^1 diffeomorphisms. We say that F_1 and F_2 are synchronously hyperbolic if they are either both order reversing, or both order preserving, and there exist $\lambda > 1$, a universal pair of cones K^u and K^s , and cone fields C^u and C^s (consisting of cones K_P^u and K_P^s , $P \in \mathbb{R}^2$, respectively) that satisfy the following properties:

(S1) For every point $P \in \mathbb{R}^2$, we have $K_P^u \subset K^u$, $K_P^s \subset K^s$, $DF_{iP}(K_P^u) \subset (K_{F_i(P)}^u)$, and

$$DF_{iP}^{-1}(K_P^s) \subset (K_{F_i^{-1}(P)}^s) \text{ for } i = 1, 2.$$

(S2) For every point $P \in \mathbb{R}^2$ and $i = 1, 2$, we have $\|DF_i(\mathbf{u})\| \geq \lambda\|\mathbf{u}\|$ for every $\mathbf{u} \in K_P^u$

and $\|DF_i^{-1}(\mathbf{w})\| \geq \lambda\|\mathbf{w}\|$ for every $\mathbf{w} \in K_P^s$.

(S3) There exists a smooth curve $\Gamma \subset \mathbb{R}^2$ such that, for every $P \in \Gamma$ we have $F_1(P) = F_2(P)$, the vector tangent to Γ at P belongs to K_P^s , and the vector tangent to $F_i(\Gamma)$ at $F_i(P)$ belongs to $K_{F_i(P)}^u$. We require that Γ is infinite in both directions.

We call Γ the divider. It divides the plane into two parts, which we call the left half-plane and the right half-plane. In addition, $F_1(\Gamma) = F_2(\Gamma)$ divides the plane into two parts, which we call the upper half-plane and the lower half-plane.

Definition 3 ([34]). Let $F_1, F_2 : \mathbb{R}^2 \rightarrow \mathbb{R}^2$ be synchronously hyperbolic C^1 diffeomorphisms with the divider Γ . Let $F : \mathbb{R}^2 \rightarrow \mathbb{R}^2$ be defined by the formula:

$$F(P) = \begin{cases} F_1(P) & \text{if } P \text{ is in the left half-plane;} \\ F_2(P) & \text{if } P \text{ is in the right half-plane.} \end{cases} \tag{11}$$

We call the map F *Lozi-like* if the following hold:

(L'.1) $-1 < \det DF_i(P) < 0$ for every point $P \in \mathbb{R}^2$ and $i = 1, 2$.

(L'.2) There exists a trapping region Δ (for the map F) that is homeomorphic to an open disk and whose closure is homeomorphic to a closed disk.

Using these new definitions of a *Lozi-like map*, Misiurewicz and Stimac [34] showed strong numerical evidence that there exist *Lozi-like maps* that have kneading sequences different to those of Lozi maps. The dynamics of such *Lozi-like maps* were modeled as an inverse limit of densely branching trees by Boronski and Stimac [37].

Kucharski again extended such a topological generalization, defining a generalized *Lozi-like family* [38] that encompasses in particular certain *Lozi-like maps*, orientation-preserving or reversing Lozi maps, or large parameter regions of two-dimensional border collision normal forms. He proved that this family possesses a strange attractor, arising as a homoclinic class. He also built a model as an inverse limit of densely branching trees for the mentioned families, extending the results of [37].

2.2.2. Geometrical Generalization: *Lozi-Type Map*

Juang and Chang [35] considered a map T of the form

$$T \begin{pmatrix} x \\ y \end{pmatrix} = \begin{pmatrix} y, \\ F(y) - b, \end{pmatrix}. \tag{12}$$

If $F(y)$ is a polynomial of degree n with a negative leading coefficient and distinct real roots, this map T will henceforth be called an *n th-degree Henon-type map*. If $F(y)$ is replaced by n -piecewise affine terms, this map T is called an *n th-degree Lozi-type map* (here, the term *degree* is given as analogous to polynomial by these authors; however it should be better to use *n th-piecewise*).

This map is defined in relation to a discrete version of a reaction–diffusion system. Juang and Chang considered several spatial entropies, particularly $h(T)$, $h_D(T)$, $h_N(T)$, (spatial entropy with respect to the Dirichlet and Neuman boundary conditions), and other special spatial entropies that they defined, and compared them.

2.2.3. Formulas Generalization

There are several generalizations of the map $\mathcal{L}_{a,b}$.

In [39], Aiewcharoen et al., motivated by (3), introduced the following system of difference equations:

$$\begin{cases} x_{n+1} = |x_n| - ay_n - b, \\ y_{n+1} = x_n - c|y_n| + d, \end{cases} \tag{13}$$

where $b > 4$.

They prove that:

- (i) All solutions converge toward the equilibrium point $(-1, -2)$. Moreover, for a large value of x_0 and y_0 , they prove that, if $b = 5$, then the solution converges toward the equilibrium point $(-1, -3)$;
- (ii) If $b = 6$, then the solution converges toward the periodic solution of period 5.

A trivial three-dimensional generalization was proposed by Mammeri and Kina [40], where the stability of its fixed points was investigated:

$$\begin{cases} x_{n+1} = 1 - bz_n + a|x_n|, \\ y_{n+1} = x_n, \\ z_{n+1} = y_n. \end{cases} \tag{14}$$

Another simple generalization was mentioned in the study by Joshi et al. [41] without analysis. Only a figure in three dimensions is plotted in the case $\alpha = 1.7$ and $\bar{\beta} = \beta = 0.08$:

$$\begin{cases} x_{n+1} = 1 - \alpha|x_n| + y_n, \\ y_{n+1} = \bar{\beta}y_n, \\ z_{n+1} = 1 - \alpha|z_n| + \beta x_n. \end{cases} \tag{15}$$

In the study by Bilal and Ramaswamy [42], the equation corresponding to the map (3) was written as (note the parameter $(1 - \nu)$ instead of b)

$$\begin{cases} x_{n+1} = 1 - a|x_n| - (1 - \nu)y_n, \\ y_{n+1} = x_n. \end{cases} \tag{16}$$

This equation was rewritten as a difference delay equation,

$$x_n = 1 - a|x_{n-1}| - (1 - \nu)x_{n-2}, \tag{17}$$

which suggests a natural generalization to higher dimensions,

$$x_n = 1 - a|x_{n-k}| - (1 - \nu)x_{n-d}. \tag{18}$$

Here, d and k are integers such that $k < d$ and $0 \leq \nu \leq 2$. The mapping is conservative when ν is 0 or 2 and is dissipative otherwise. For $\nu = 1$, the map reduces to a k -dimensional endomorphism, whereas, for $\nu \neq 1$, the map is a d -dimensional diffeomorphism.

A bifurcation analysis and an investigation of the dynamics through both numerical and analytical approaches were carried out in this article. Moreover, a smooth approximation of (18) was obtained by replacing the absolute value function $|\cdot|$ with a smooth function $S_\epsilon(\cdot)$:

$$x_n = 1 - aS_\epsilon(x_{n-k}) - (1 - \nu)x_{n-d}, \tag{19}$$

$$S_\epsilon(x_{n-k}) = \begin{cases} x_{n-k}^2 \setminus 2\epsilon + \epsilon \setminus 2 & \text{if } |x_{n-k}| \leq \epsilon, \\ |x_{n-k}| & \text{if } |x_{n-k}| \geq \epsilon, \end{cases} \tag{20}$$

where $0 < \epsilon < 1$.

This smooth approximation of the map enables the analysis of the bifurcations vis-a-vis the bifurcations to the generalized Hénon map. It shows that some of the bifurcations observed persist on both the piecewise Lozi and Hénon map. This kind of smoothing was previously introduced by Lozi [43] in 1979.

This generalized Lozi map (17) was also studied by Chutani et al. [44], who analyzed the time series obtained from different dynamical regimes of evolving maps and flows by constructing their equivalent time series networks using the visibility algorithm. They focused on the three-dimensional Lozi map (with $d = 3, k = 2$) that displays hyperchaotic dynamical behavior at certain parameter values, particularly at $(a, \nu) = (1.3, 0.6)$ (see Section 3.1).

Another kind of generalization was carried out by Lopesino et al. [31], who defined a *non-autonomous Lozi map* as the map.

$$L_n(x, y) = (1 + y - a(n)|x|, -x), \tag{21}$$

where $a(n) = a + \epsilon(1 + \cos(n))$, $a > 4$. They proved the existence of a chaotic saddle in the square

$$\mathcal{S}_n = \left\{ (x, y) \in \mathbb{R}^2 \mid |x| \leq R, |y| \leq R \right\},$$

with

$$R = \sup_{n \in \mathbb{N}} \frac{a(n)}{4(a(n) - 2)}$$

(see (10) for comparison).

2.2.4. Fractal Mappings

The new paradigm of *fractional mappings* recently explored is a natural extension of the theory of *fractal ordinary differential equations*.

In Khennaoui et al. [45], using the Caputo-like delta difference

$$\begin{aligned} {}^c \Delta_a^\nu X(t) &= \Delta_a^{-(n-\nu)} \Delta^n X(t), \\ &= \frac{1}{\Gamma(n-\nu)} \sum_{s=a}^{t-(n-\nu)} (t-s-1)^{(n-\nu-s)} \Delta^n X(t) \end{aligned}$$

the fractal Lozi map was defined as:

$$\begin{cases} {}^c\Delta_a^\nu x(t) &= \alpha|x(t-1+\nu)| + y(t-1+\nu) + 1 - x(t-1+\nu), \\ {}^c\Delta_a^\nu y(t) &= \beta x(t-1+\nu) - y(t-1+\nu), \end{cases} \tag{22}$$

for $0 < \nu \leq 1$ and $t \in \mathbb{N}_{a+1-\nu}$. One can note that the fractional order of both fractional differences are identical, leading to what is commonly referred to as a commensurate system. An equivalent discrete integral equation of such a map is obtained:

$$\begin{cases} x(t) &= x(a) + \frac{1}{\Gamma(\nu)} \sum_{s=a+1}^{t-\nu} (t-s-1)^{(\nu-1)} (-\alpha|x(t-1+\nu)| + y(t-1+\nu) + 1 - x(t-1+\nu)), \\ y(t) &= y(a) + \frac{1}{\Gamma(\nu)} \sum_{s=a-\nu}^{t-\nu} (t-s-1)^{(\nu-1)} (\beta x(t-1+\nu) - y(t-1+\nu)), \end{cases} \tag{23}$$

where $\frac{(t-s-1)^{(\nu-1)}}{\Gamma(\nu)}$ is the discrete kernel function

$$\frac{(t-s-1)^{(\nu-1)}}{\Gamma(\nu)} = \frac{\Gamma(t-s)}{\Gamma(\nu)\Gamma(t-s-\nu+1)},$$

and $a = 0$ yields the numerical formula

$$\begin{cases} x(n) &= x(0) + \frac{1}{\Gamma(\nu)} \sum_{j=1}^n \frac{\Gamma(n-j+\nu)}{\Gamma(n-j+1)} (-\alpha|x(j-1)| + y(j-1) + 1 - x(j-1)), \\ y(n) &= y(0) + \frac{1}{\Gamma(\nu)} \sum_{j=1}^n \frac{\Gamma(n-j+\nu)}{\Gamma(n-j+1)} (\beta x(j-1) - y(j-1)). \end{cases} \tag{24}$$

A complete numerical analysis of this fractional map shows that the value of the fractional order ν affects the bifurcation diagram (of the non-fractional map) both in terms of its general shape and the duration of the chaotic interval. For $\nu = 0.98$, the bifurcation diagram is similar to the corresponding integer diagram except for a small broadening in the interval where the chaos is observed. As ν decreases further, it is found that, when $0 \leq \alpha \leq 0.5$, the orbit no longer goes to a fixed point. In fact, as n increases, one observes that the trajectory becomes unbounded. A major difference between the bifurcation diagram of the integer and fractional maps is in the interval over which chaos is observed. The interval becomes slightly smaller as ν decreases.

A combined Hénon–Lozi fractional map was defined using a linear interpolation of quadratic and absolute value functions and studied by Ibrahim and Baleanu [46].

2.2.5. Non-Conventional Generalization

A non-conventional generalization of (3) based on the cosine chaotic map has recently been published [47]. The cosine chaotic map (CCM) is the chaotification method that enhances the chaotic complexity of the existing chaotic maps. This method performs the cosine function alongside a chaotic map that cascades in the used system. Thus, the results provide a new chaotic map with a wide chaotic range within the closed interval $[-1, +1]$. Theoretically, the CCM has properties based on the properties of the underlying seed maps. In the case of the Lozi map, Aliwi and Ajeena considered (3), changing 1 to 3 in the first component

$$f \begin{pmatrix} x \\ y \end{pmatrix} = \begin{pmatrix} 3 - a|x| + y, \\ bx, \end{pmatrix} \tag{25}$$

with $a = -1.8$ and $b = 0.25$. Then, they inserted (25) into the CCM:

$$f \begin{pmatrix} x \\ y \end{pmatrix} = \begin{pmatrix} \cos \left(2^{(k+3-a|x|+y)} \right), \\ \cos \left(2^{(k+bx)} \right), \end{pmatrix} \tag{26}$$

where $k \in [10, 24]$.

Starting with any initial point (x_0, y_0) belonging to the basin of attraction of the Lozi map, the iterates randomly fulfill the square $[-1, +1]^2$ (see Figure 8).

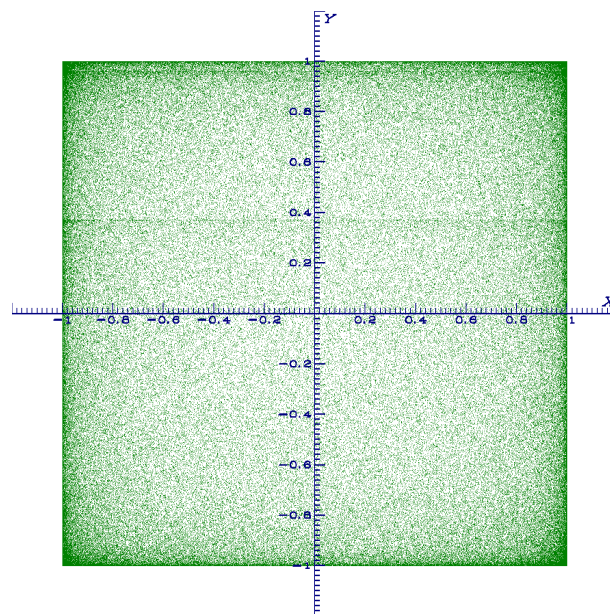


Figure 8. Image on the (x, y) -plane of 300,000 iterates of the cosine Lozi chaotic map (26). Initial value $(x_0 = 0.1, y_0 = 0.3)$.

This generalized map is built for cryptographic purposes. In [48], these authors, for the same purpose, combined the Lozi map with the sine function instead:

$$f \begin{pmatrix} x \\ y \end{pmatrix} = \begin{pmatrix} \sin \left(2^{(k+3-a|x|+y)} \right) \\ \sin \left(2^{(k+bx)} \right) \end{pmatrix} \tag{27}$$

2.2.6. Network of Chaotic Maps and Chimera

Besides the generalizations presented above, the Lozi map can be used to construct networks of chaotic attractors, either alone or with the Hénon map.

Cano and Cosenza [49] considered the autonomous system of globally coupled Lozi maps described by the equations

$$\begin{cases} x_{n+1}^i = (1 - \epsilon)f(x_n^i, y_n^i) + \epsilon h_n, \\ y_{n+1}^i = bx_n^i, \end{cases} \tag{28}$$

with $f(x_n, y_n) = 1 - a|x_n| + y_n$ and $h_n = \frac{1}{N} \sum_{j=1}^N f(x_n^j, y_n^j)$. The parameter ϵ represents the strength of the global coupling of the maps.

Synchronization in this system of equations at the iterate n arises when $(x_n^i, y_n^i) = (x_n^j, y_n^j), \forall (i, j)$. Note that the synchronization of the x variable implies the synchronization of the y variable. Besides synchronization, the following collective states can be defined in this globally coupled system:

- (i) *Clustering.* A dynamical cluster is defined as a subset of elements that are synchronized among themselves. In a clustered state, the elements in the system segregate into K distinct subsets that evolve in time, i.e., $x_n^i = x_n^j = X_n^v, \forall (i, j)$ in the v th cluster with $v = 1, \dots, K$.
- (ii) A *chimera state* consists of the coexistence of one or more clusters and a subset of desynchronized elements.
- (iii) A *desynchronized or incoherent state* occurs when $x_n^i \neq x_n^j, \forall (i, j)$.

They also considered the system of nonlocally coupled Lozi maps described by

$$\begin{cases} x_{n+1}^i = (1 - \epsilon)f(x_n^i, y_n^i) + \epsilon h_n, \\ y_{n+1}^i = b x_n^i, \end{cases} \quad (29)$$

with

$$h_n^i = \frac{1}{2k} \sum_{j=i-k}^{j=i+k} [f(x_n^i, y_n^i) - f(x_n^j, y_n^j)], \quad (30)$$

where the elements $i = 1, \dots, N$ are located on a ring with periodic boundary conditions, ϵ is the coupling parameter, k is the number of neighbors coupled on either side of site i , and h_n^i is the local field acting on element i .

The presence of chimera states in globally coupled networks of identical oscillators at first seemed counterintuitive because of the perfect symmetry of such a system. However, such networks are among the simplest extended systems that can exhibit chimera behavior. Cano and Cosenza highlighted that the presence of global interactions can indeed allow for the emergence of chimera states in networks of coupled elements possessing chaotic hyperbolic attractors, such as Lozi maps, where such states do not form with local interactions. Both chimeras and clusters can be interpreted as manifestations of the multistability of the resulting drive-response dynamics at the local level in systems with global interactions. Their results suggest that chimera states, as other collective behaviors, arise from the interplay between the local dynamics and the network topology; either ingredient can prevent or induce its occurrence.

Semenova et al. [50] studied a slight variant of (29):

$$\begin{cases} x_{n+1}^i = f(x_n^i, y_n^i) + \frac{\sigma}{2P} \sum_{j=i-P}^{j=i+P} [f(x_n^j, y_n^j) - f(x_n^i, y_n^i)], \\ y_{n+1}^i = b x_n^i, \end{cases} \quad (31)$$

$i = 1, 2, \dots, N$, where N is the number of elements in the ensemble of coupled equations. The nonlocal coupling is characterized by the coupling strength σ , the number of neighbours $2P$ (P neighbors on either side of the i th element), and the coupling range $r = P/N$.

They show that the ensemble of nonlocally coupled Lozi maps demonstrates the solitary state for specific values of coupling parameters. The coupling changes the properties of partial elements and leads to the bistability, though the Lozi map does not have this property in the uncoupled form. The emergence of solitary states is accompanied by the arising of the second attracting set for the ensemble element.

Other examples of chimera states were exhibited by Anishchenko et al. [51], who numerically explored the dynamics of two coupled one-dimensional ensembles: an ensemble of Hénon maps and an ensemble of Lozi maps. Both networks are considered under conditions of non-local coupling. The ensemble of Lozi maps was characterized by a hyperbolic attractor of the individual elements, whereas the ensemble of Hénon maps was characterized by a non-hyperbolic attractor. They revealed the features of realizing chimera states in the coupled system, which are caused by the mutual influence of two ensembles with fundamentally different dynamics without coupling.

3. Three-Dimensional Hyperchaotic Attractors

A hyperchaotic attractor of a discrete dynamical system is usually defined as a chaotic behavior with at least two positive Lyapunov exponents. Combined with one negative exponent to ensure the convergence of the iterates toward the attractor, the minimal dimension for a discrete hyperchaotic system is three. Therefore, for a continuous dynamical system, four ordinary differential equations (ODEs) are required.

3.1. Rössler Hyperchaotic Attractors

In 1979, Rössler proposed several examples of systems of four ODEs and 3D mappings providing hyperchaos. Two of them are presented in this section.

3.1.1. The “Noodle” Attractor

First, in [52],

$$\begin{cases} x_{n+1} = -ax_n(1 - x_n^2) - y_n - z_n, \\ y_{n+1} = bx_n, \\ z_{n+1} = c(z_n^2 - 0.33) + dz_n, \end{cases} \tag{32}$$

with $a = 2.7, b = 0.09, c = 0.09,$ and $d = 0.4$.

The projection of this attractor (see Figure 9) onto the (x, y) -plane looks like “folded noodles” as said by Rössler himself, which indicates that this kind of attractor possesses only “one direction of lateral expansion”.

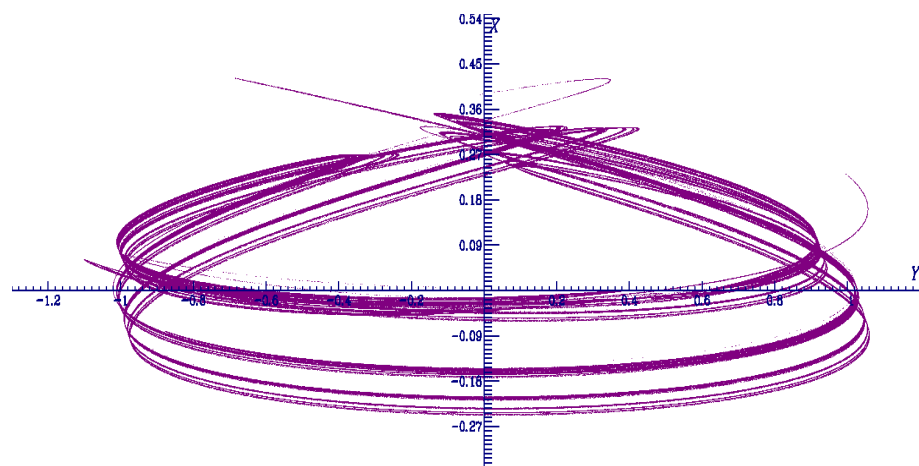


Figure 9. Projection onto the (x, y) -plane of the 3D Rössler “noodle” hyperchaotic attractor (32). Initial value $(x_0 = 0, y_0 = 0.2, z_0 = 0)$.

3.1.2. The Folded “Curtain” Attractor

Second, in [53], there is the following:

$$\begin{cases} x_{n+1} = 3.4x_n(1 - x_n) - 0.05(y_n + 0.35)(1 - 2z_n), \\ y_{n+1} = 0.1[(y_n + 0.35)(1 - 2z_n) - 1](1 - 1.9x_n), \\ z_{n+1} = 3.78z_n(1 - z_n) + 0.01y_n. \end{cases} \tag{33}$$

The projection of this attractor (see Figure 10) onto the (y, x) -plane looks like a folded curtain.

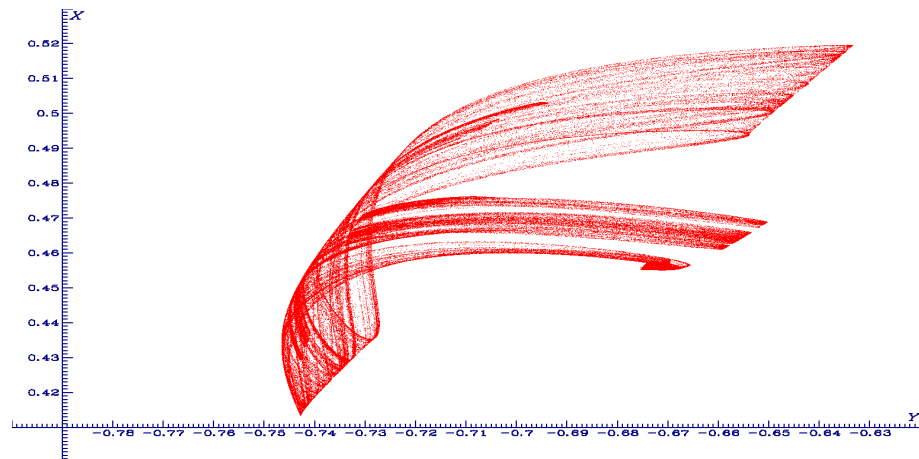


Figure 10. Projection onto the (y, x) -plane of the 3D Rössler “curtain” hyperchaotic attractor (33). Initial value $(x_0 = 0.1, y_0 = 0.1, z_0 = 0.1)$.

3.2. Three-Dimensional Lozi Map with Coexistence of Thread and Sheet Hyperchaotic Attractor

The most important features of the classical Lozi map $\mathcal{L}_{a,b}$ (3) are its simplicity and piecewise linearity, which make formal calculus easily tractable. The previous examples of Rössler (32), (33), both with a third-order nonlinearity and with five and nine parameters, cannot be analyzed analytically nor thoroughly by numerical computation. That is why, in this section, one introduces a much simpler example of hyperchaos based on the use of piecewise linearity. Moreover, one wants to conserve another essential feature of the Lozi map: the determinant of the Jacobian matrix ought to be constant. This is a tough condition that implies defining a non-continuous mapping. However, there are several advantages for keeping such a determinant constant, such as assuming hyperbolicity.

As pointed out in [17], in two dimensions, the main advantage of the Lozi map over the Hénon map is that one can prove hyperbolicity without much effort. This is the main reason why so little is known for the Hénon map, where hyperbolicity is believed to occur only on Cantor-like sets of parameters. The Lozi map is rather similar to Sinai’s billiards; in particular, the discontinuity of the differential allows for the uniform hyperbolicity as in the billiards case. The uniformly hyperbolic attractors were introduced in mathematical theory on dynamical systems due to Smale, Anosov, Sinai, and other researchers in the 1960s–1970s [54]. Hyperbolic attractors are characterized by roughness or structural stability. In the context of physical or technical objects, this implies an insensitivity of the dynamical behavior to small variations in parameters, manufacturing imperfections, interferences, etc. This may be significant for possible applications [55]. It turned out, however, that hyperbolic chaos is not widespread in real-world systems, and its implementation requires special efforts [56].

Hence, the proposed *thread–sheet* hyperchaotic attractor is

$$\begin{cases} x_{n+1} = a|x_n| + y_n \operatorname{sgn}(z_n) + 1, \\ y_{n+1} = b(x_n + z_n), \\ z_{n+1} = y_n \operatorname{sgn}(x_n) + c|z_n| + 1, \end{cases} \tag{34}$$

also represented by the iterates of any initial point $(x_0, y_0, z_0)^T$ by the map $T_{a,b,c} : \mathbb{R}^3 \rightarrow \mathbb{R}^3$:

$$T_{a,b,c} \begin{pmatrix} x \\ y \\ z \end{pmatrix} = \begin{pmatrix} a|x| + y \operatorname{sgn}(z) + 1, \\ b(x + z), \\ y \operatorname{sgn}(x) + c|z| + 1, \end{pmatrix} \tag{35}$$

with $\operatorname{sgn}(x) = 1$ if $x \geq 0$, and $\operatorname{sgn}(x) = -1$ if $x < 0$.

The particularity of this map is that one can observe, for many values of the parameters (when $a = c$), the coexistence of two chaotic attractors with a different dimensionality: a

thread-strange attractor that belongs to the plane (x, z) and a *sheet*-strange attractor with a three-dimensional structure. This *thread* chaotic attractor is a combination of straight lines; instead, the *sheet* chaotic attractor seems to be made of many planes (see Figures 11 and 12).

One can find some analogy in dimensionality between the *thread* chaotic attractor and the “noodle attractor” proposed by Rössler (32) on the one hand, and on the other hand, between the *sheet* chaotic attractor and its folded “curtain” chaotic attractor (33).

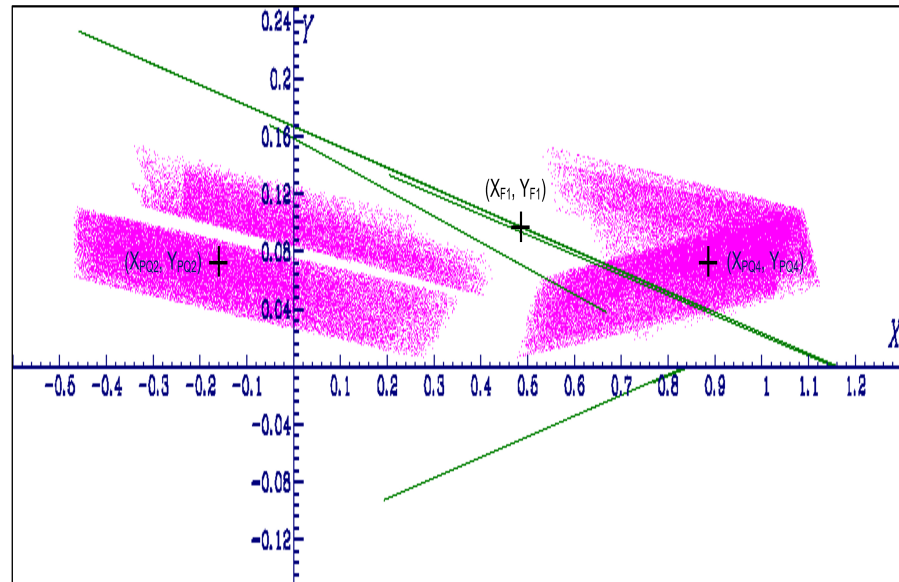


Figure 11. Projection onto the (x, y) -plane of the coexisting *sheet* and *thread* 3D Lozi map (35) hyperchaotic attractors for the parameter value $a = -1.25, b = 0.1, c = -1.25$. Initial value of the *thread*-attractor (in green) $(x_0 = 0.1, y_0 = 0.2, z_0 = 0.1)$. Initial value of the *sheet*-attractor (in purple) $(x_0 = 0.11, y_0 = 0.2, z_0 = 0.1)$.

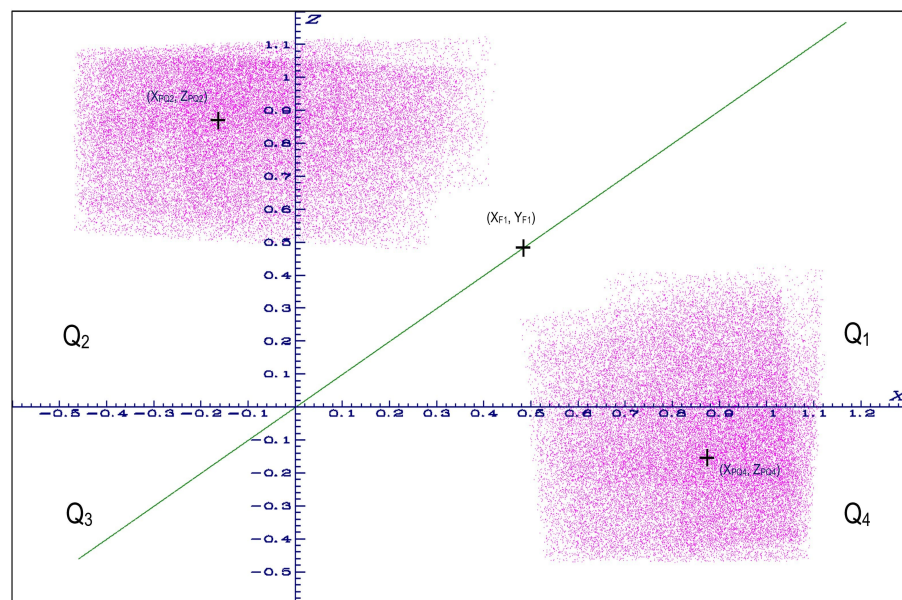


Figure 12. Projection onto the (x, z) -plane of the coexisting *sheet* and *thread* 3D Lozi map (35) hyperchaotic attractors for the parameter value $a = -1.25, b = 0.1, c = -1.25$. Initial value of the *thread*-attractor (in green) $(x_0 = 0.1, y_0 = 0.2, z_0 = 0.1)$. Initial value of the *sheet*-attractor (in purple) $(x_0 = 0.11, y_0 = 0.2, z_0 = 0.1)$.

In this article, we keep the name *sheet* chaotic attractor even if its structure is more complicated (see Figures 13 and 14).

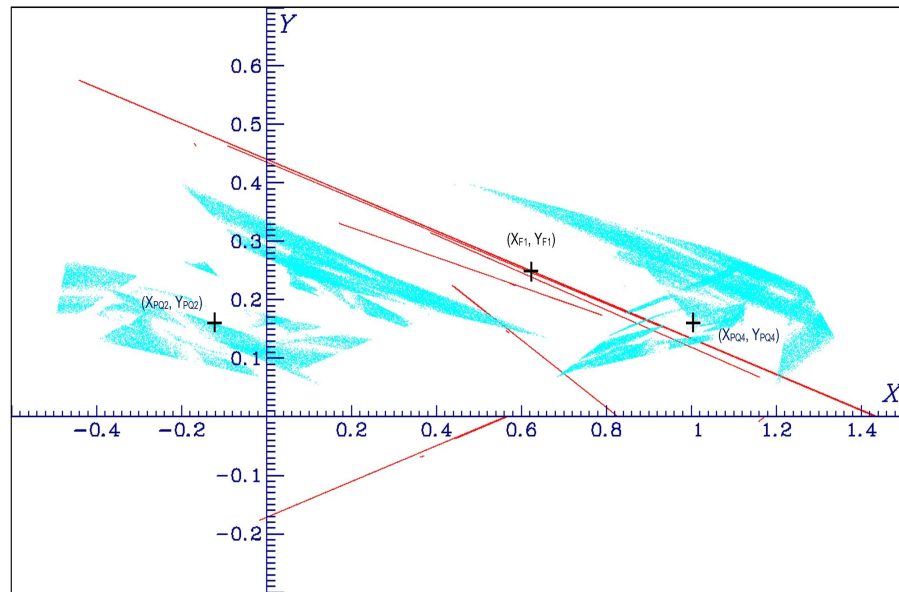


Figure 13. Projection onto the (x, y) -plane of the coexisting *sheet* and *thread* 3D Lozi map (35) hyperchaotic attractors for the parameter value $a = -1.0, b = 0.2, c = -1.0$. Initial value of the *thread*-attractor (in red) $(x_0 = 0.1, y_0 = 0.2, z_0 = 0.1)$. Initial value of the *sheet*-attractor (in cyan) $(x_0 = 0.11, y_0 = 0.2, z_0 = 0.1)$.

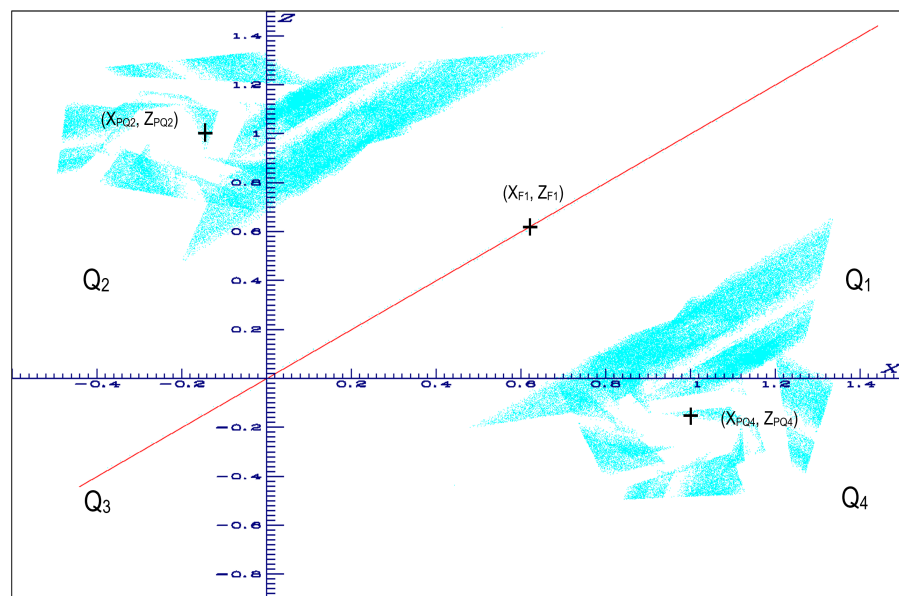


Figure 14. Projection onto the (x, z) -plane of the coexisting *sheet* and *thread* 3D Lozi map (35) hyperchaotic attractors for the parameter value $a = -1.0, b = 0.2, c = -1.0$. Initial value of the *thread*-attractor (in red) $(x_0 = 0.1, y_0 = 0.2, z_0 = 0.1)$. Initial value of the *sheet*-attractor (in cyan) $(x_0 = 0.11, y_0 = 0.2, z_0 = 0.1)$.

4. Properties of Thread-Sheet Hyperchaotic Attractor

In this section, some properties of $T_{a,b,c}$ are given. Even if the piecewise linear functions composing this map allow us to perform explicit calculations, there is a need for a huge amount of studies to completely understand its dynamics. One can compare this situation with the studies on the Lozi map, for which, 46 years after its discovery, important features

are still discovered (see, for example, the Ph. Thesis of Kilassa Kvaternik [57] in 2022 on the tangential homoclinic points locus of $\mathcal{L}_{a,b}$).

4.1. Basic Properties: Jacobian and Symmetry

The map $T_{a,b,c}$ (35) is much simpler than the hyperchaotic maps proposed by Rössler (32), (33). It is also different from generalizations of the Lozi map described in Section 2.2.3. For convenience, henceforth, the following notation of $T_{a,b,c}$ is used:

$$T_{a,b,c} \begin{pmatrix} x \\ y \\ z \end{pmatrix} = \begin{pmatrix} a_X x + 1_Z y + 1, \\ b(x + z), \\ 1_X y + c_Z z + 1, \end{pmatrix}, \tag{36}$$

with $a_X = a \operatorname{sgn}(x)$, $c_Z = c \operatorname{sgn}(z)$ (because $a_X x = a|x|$ and $c_Z z = c|z|$), $1_X = \operatorname{sgn}(x)$, and $1_Z = \operatorname{sgn}(z)$.

If $x \neq 0$ and $z \neq 0$, the Jacobian matrix $J_{a,b,c}$ of $T_{a,b,c}$ is definite

$$J_{a,b,c} \begin{pmatrix} x \\ y \\ z \end{pmatrix} = \begin{pmatrix} a_X & 1_Z & 0 \\ b & 0 & b \\ 0 & 1_X & c_Z \end{pmatrix}, \tag{37}$$

and, as $1_X a_X = a$ and $1_Z c_Z = c$, its determinant is

$$\operatorname{Det} J_{a,b,c} = -b(a + c).$$

Therefore, the map is dissipative and can have an attractor if and only if

$$-1 < -b(a + c) < 1. \tag{38}$$

It is interesting to note that there is a symmetry conjugating parameters and variables

$$T_{a,b,c}(x, y, z) = T_{c,b,a}(z, y, x). \tag{39}$$

4.2. The Thread-Attractor

If $a = c$, there is a special projection of (36) in the plane $(x = z, y)$ that reduces the map $T_{a,b,c}$ to $T_{a,b}$:

$$T_{a,b} \begin{pmatrix} x \\ y \end{pmatrix} = \begin{pmatrix} a_X x + 1_X y + 1, \\ 2bx. \end{pmatrix} \tag{40}$$

This map is a 2D chaotic attractor, which is the *thread*-attractor observed in Figures 11–14. Its structure is fractal as shown in Figure 15.

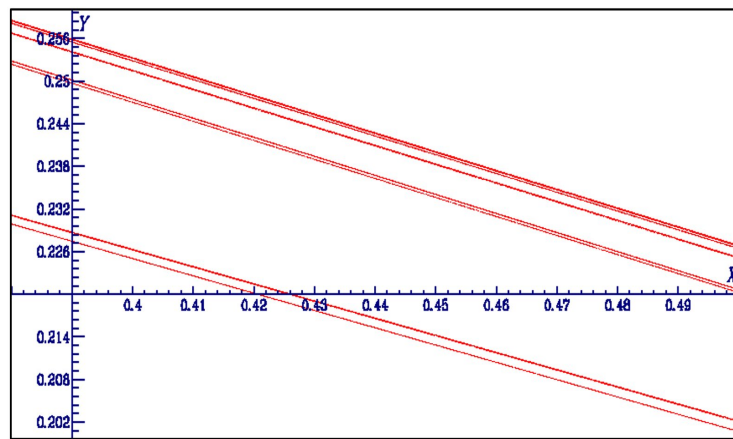


Figure 15. Magnification of Figure 16 on the $(x = z, y)$ -plane of the *thread*-attractor, showing its fractal structure. Parameter value $a = -1.0, b = 0.2, c = -1.0$, initial value of the *thread*-attractor $(x_0 = 0.1, y_0 = 0.2, z_0 = 0.1)$.

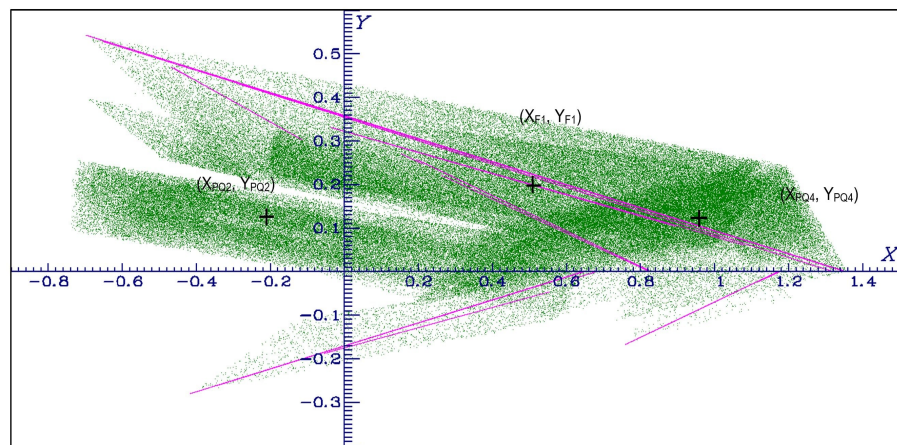


Figure 16. Projection onto the (x, y) -plane of the coexisting *sheet* and *thread* 3D Lozi map (35) hyperchaotic attractor for the parameter value $a = -1.25, b = 0.2, c = -1.25$. Initial value of the *thread*-attractor (in purple) $(x_0 = 0.1, y_0 = 0.1, z_0 = 0.1)$. Initial value of the *sheet*-attractor (in green) $(x_0 = 0.1, y_0 = 0.2, z_0 = 0.1)$.

4.3. Fixed Points and Period-Two Orbits

As seen in Section 2.1.3, fixed points play an important role in shaping the chaotic attractors and their basin of attraction. In the following, the plane (x, z) is divided into four quadrants: $Q_1 = \{x \geq 0, z \geq 0\}$, $Q_2 = \{x < 0, z \geq 0\}$, $Q_3 = \{x < 0, z < 0\}$, $Q_4 = \{x \geq 0, z < 0\}$.

The fixed points of $T_{a,b,c}$ are obtained, solving the system

$$T_{a,b,c} \begin{pmatrix} x \\ y \\ z \end{pmatrix} = \begin{pmatrix} x \\ y \\ z \end{pmatrix}, \tag{41}$$

whose solutions are:

$$\begin{cases} x_F = \frac{1 - c_{Z_F} - b_{X_F} + b_{Z_F}}{\Delta}, \\ y_F = \frac{b(2 - a_{X_F} - c_{Z_F})}{\Delta}, \\ z_F = \frac{1 - a_{X_F} - b_{Z_F} + b_{X_F}}{\Delta}, \end{cases} \tag{42}$$

where

$$\Delta = a_{X_F} c_{Z_F} + b(a - 1_{Z_F} - 1_{X_F} + c) + 1 - c_{Z_F} - a_{X_F},$$

with $b_{x_F} = b1_{x_F}, b_{z_F} = b1_{z_F}$, provided the sign of x_F and z_F are in accordance with those of the coefficients in the quadrant where the solution belongs (see example below and in Section 4.4). This implies that there can exist at most (but not always) four fixed points (one in each quadrant) instead of only two for the 2D Lozi map.

The related eigenvalues of the Jacobian are the roots of the characteristic polynomial

$$P(\lambda) = -\lambda^3 + \lambda^2(a_X + c_Z) + \lambda(b(1_X + 1_Z)a_Xc_Z) - b(a + c). \tag{43}$$

As an example, the fixed point in the quadrant Q_1 is

$$\begin{cases} x_{F_1} = \frac{1-c}{\Delta}, \\ y_{F_1} = \frac{b(2-a-c)}{\Delta}, \\ z_{F_1} = \frac{1-a}{\Delta}, \end{cases} \tag{44}$$

with $\Delta = ac + b(a + c - 2) + 1 - c - a$, because $1_{x_{F_1}} = 1 = 1_{z_{F_1}}$ and $b_{x_{F_1}} = b = b_{z_{F_1}}$.

For some parameter values such as those of Figures 11–14, it seems that the chaotic attractor is generated by the unstable invariant manifold of a period-two orbit belonging to Q_4 and Q_2 . The piecewise linear form of (36) allows us to compute the periodic orbit of any period. In the case of period-two with $(x_{PQ_2}, z_{PQ_2}) \in Q_2$ and $(x_{PQ_4}, z_{PQ_4}) \in Q_4$, the value of $(x_{PQ_4}, y_{PQ_4}, z_{PQ_4})$ is obtained solving the system

$$\begin{cases} (-a^2 + b - 1)x_{PQ_4} + ay_{PQ_4} + bz_{PQ_4} = a - 1, \\ abx_{PQ_4} - y_{PQ_4} - bcz_{PQ_4} = -2b, \\ bx_{PQ_4} - cy_{PQ_4} + (b + c^2 + 1)z_{PQ_4} = c + 1, \end{cases} \tag{45}$$

which gives the solution

$$\begin{cases} x_{PQ_4} = \frac{a-2ab^2-ab-2b+ac^2-bc^2-c^2-2b^2c+abc-bc-1}{\Delta}, \\ y_{PQ_4} = \frac{-a^2b^2-2ab^2-ab^2-ab-2b+b^2c^2-abc^2-bc^2-2b^2c+a^2bc+bc}{\Delta}, \\ z_{PQ_4} = \frac{-a^2+2ab^2+a^2b-ab+2b-a^2c+2bc^2-abc-bc-c-1}{\Delta}, \end{cases} \tag{46}$$

with $\Delta = b^2(a + c)^2 - (a^2 + c^2 + a^2c^2) - 1$, provided that $\Delta \neq 0$ and the condition $(x_{PQ_4}, z_{PQ_4}) \in Q_4$ depending on the parameter values is verified. Then,

$$x_{PQ_2} = z_{PQ_4}, y_{PQ_2} = y_{PQ_4}, z_{PQ_2} = x_{PQ_4}.$$

4.4. Numerical Examples

This new three-dimensional mapping can generate a large variety of chaotic and hyperchaotic attractors. We give five examples of such behavior in this section. In the first three examples, there is the coexistence of *thread* and *sheet* chaotic attractors. However, their shapes are different and they are constituted by a different number of pieces. In the two last examples, the blow up of the attractors with respect to parameter a and b is highlighted.

4.4.1. Case $a = -1.25, b = 0.1, c = -1.25$, One-Piece Chaotic Attractor, Two-Piece Hyperchaotic Attractor

The value of the Jacobian is 0.25. In this case, there exist four fixed points: two of them are in the plane $(x = z, y)$ and are related to the *thread*-attractor.

In Q_1 , the fixed point belongs to the plane $x = z$ (see Figures 11 and 12):

$$x_{F_1} = z_{F_1} = 20/41 \approx 0.487804, y_{F_1} = 4/41 \approx 0.097560,$$

The corresponding eigenvalues of the Jacobian matrix are

$$\lambda_1 \approx -1.393521, \lambda_2 = -1.25, \lambda_3 \approx +0.143521.$$

Hence, the dimension of the unstable invariant manifold in \mathbb{R}^3 of this fixed point $(x_{F_1}, y_{F_1}, z_{F_1})$ is two (and that of the stable invariant manifold is one). However, in the plane $(x = z, y)$, the map $T_{a,b}$ (40) has only two eigenvalues:

$$\lambda_1 \approx -1.393521, \lambda_2 = +0.143521.$$

Therefore, in this plane, the unstable invariant manifold of the fixed point (x_{F_1}, y_{F_1}) is only one-dimensional, like the stable invariant manifold. This unstable invariant manifold nests the skeleton of the *thread* chaotic attractor (see Figure 11).

In Q_3 , the fixed point also belong to the plane $x = z$:

$$x_{F_3} = z_{F_3} = -20, y_{F_3} = -4.$$

The corresponding eigenvalues of the Jacobian matrix are

$$\lambda_1 \approx +1.06161, \lambda_2 = +1.25, \lambda_3 \approx +0.188394.$$

Hence, the dimension of the unstable invariant manifold in \mathbb{R}^3 of this fixed point $(x_{F_1}, y_{F_1}, z_{F_1})$ is two (and that of the stable invariant manifold is one). However, in the plane $(x = z, y)$, the map $T_{a,b}$ (40) has only two eigenvalues:

$$\lambda_1 \approx +1.06161, \lambda_2 = +0.188394.$$

Therefore, in this plane, the unstable invariant manifold of the fixed point (x_{F_3}, y_{F_3}) is only one-dimensional, like the stable invariant manifold. Analogous with the results displayed in Section 2.1.3, it is reasonable to think that the invariant stable manifold of (x_{F_3}, y_{F_3}) allows us to define the boundary of the basin of attraction of the *thread*-attractor. However, this point remains to be proven (see, for example, Figure 1.2 of [57] regarding the complicated shape of the stable and unstable manifold of the unstable fixed point of $\mathcal{L}_{a,b}$ for the values $a = 1.46, b = 0.86$).

The other two fixed points (x_{F_2}, y_{F_2}) and (x_{F_4}, y_{F_4}) belong to Q_2 and Q_4 .

$$x_{F_2} = \frac{-2.45}{0.8125} \approx -3.015385, y_{F_2} = \frac{-0.2}{0.8125} \approx -0.246154, z_{F_2} = \frac{0.45}{0.8125} \approx 0.553846,$$

and

$$x_{F_4} = \frac{0.45}{0.8125} \approx 0.553846, y_{F_4} = \frac{-0.2}{0.8125} \approx -0.246154, z_{F_4} = \frac{-2.45}{0.8125} \approx -3.015385.$$

One can remark the symmetry:

$$x_{F_2} = z_{F_4}, y_{F_2} = y_{F_4}, z_{F_2} = x_{F_4}.$$

The corresponding eigenvalues of the Jacobian matrix of the fixed points $(x_{F_2}, y_{F_2}, z_{F_2})$, and $(x_{F_4}, y_{F_4}, z_{F_4})$ are

$$\lambda_1 \approx +1.32341, \lambda_2 = +0.162759, \lambda_3 \approx -1.16065.$$

There also exists a period-two orbit of the type discussed in the previous section:

$$x_{PQ_4} = \frac{196}{225} \approx 0.871111, y_{PQ_4} = \frac{16}{225} \approx 0.071111, z_{PQ_4} = \frac{-4}{225} = -0.16;$$

$$x_{PQ_2} = z_{PQ_4}, y_{PQ_2} = y_{PQ_4}, z_{PQ_2} = x_{PQ_4}.$$

It seems that each piece of this *sheet* hyperchaotic attractor is linked to one component of the period-two orbit (see Figures 11 and 12).

Moreover, there does not exist a period-two orbit going from Q_1 to Q_3 and vice-versa.

4.4.2. Case $a = -1.0, b = 0.2, c = -1.0$, Multi-Pieces Chaotic and Hyperchaotic Attractor

The value of the Jacobian is 0.4. In this case, there exist only three fixed points; one of them is in the plane $(x = z, y)$ and is related to the *thread*-attractor (see Figures 13 and 14).

$$x_{F_1} = z_{F_1} = 5/8 = 0.625, y_{F_1} = 1/4 = 0.25.$$

The eigenvalues of the Jacobian matrix are

$$\lambda_1 \approx -1.306226, \lambda_2 = -1.0, \lambda_3 \approx +0.306226.$$

Hence, the dimension of the unstable invariant manifold of this fixed point is one (and that of the stable invariant manifold is one). However, in the plane $(x = z, y)$, the map (40) has only two eigenvalues:

$$\lambda_1 \approx -1.306226, \lambda_2 = +0.306226.$$

Therefore, in this plane, the unstable invariant manifold of this fixed point is only one-dimensional like for the stable manifold. This unstable invariant manifold is the skeleton of the *thread*-attractor (see Figure 13).

However, in Q_3 , there is no fixed point. Therefore, the boundary of the basin of attraction of the thread chaotic attractor cannot be linked to a second fixed point in the plane.

The other two fixed points (x_{F_2}, y_{F_2}) and (x_{F_4}, y_{F_4}) belong to Q_2 and Q_4 :

$$x_{F_2} = -6, y_{F_2} = -1, z_{F_2} = 1,$$

and

$$x_{F_4} = 1, y_{F_4} = -1, z_{F_4} = -6.$$

One can again remark the symmetry:

$$x_{F_2} = z_{F_4}, y_{F_2} = y_{F_4}, z_{F_2} = x_{F_4}.$$

There also exists a period-two orbit of the type discussed in the previous section:

$$x_{PQ_4} = 1, y_{PQ_4} = 1/6 \approx 0.16666, z_{PQ_4} = -1/6 \approx -0.16666;$$

$$x_{PQ_2} = z_{PQ_4}, y_{PQ_2} = y_{PQ_4}, z_{PQ_2} = x_{PQ_4}.$$

In this case, the geometry of the multi-piece hyperchaotic attractor is more complicated than that of the previous case, even if the period-two orbit belongs to it (see Figures 13 and 14).

4.4.3. Case $a = -1.25, b = 0.2, c = -1.25$, Connected Hyperchaotic Attractor

The value of the Jacobian is 0.5. In this case, there exist only three fixed points; one of them is in the plane $(x = z, y)$ and is related to the *thread*-attractor (see Figures 16 and 17).

$$x_F = 20/37 \approx 0.54054 = z_F, y_F = 8/37 \approx 0.21622.$$

The eigenvalues of the Jacobian matrix are

$$\lambda_1 \approx -1.514171, \lambda_2 = -1.25, \lambda_3 \approx +0.264171.$$

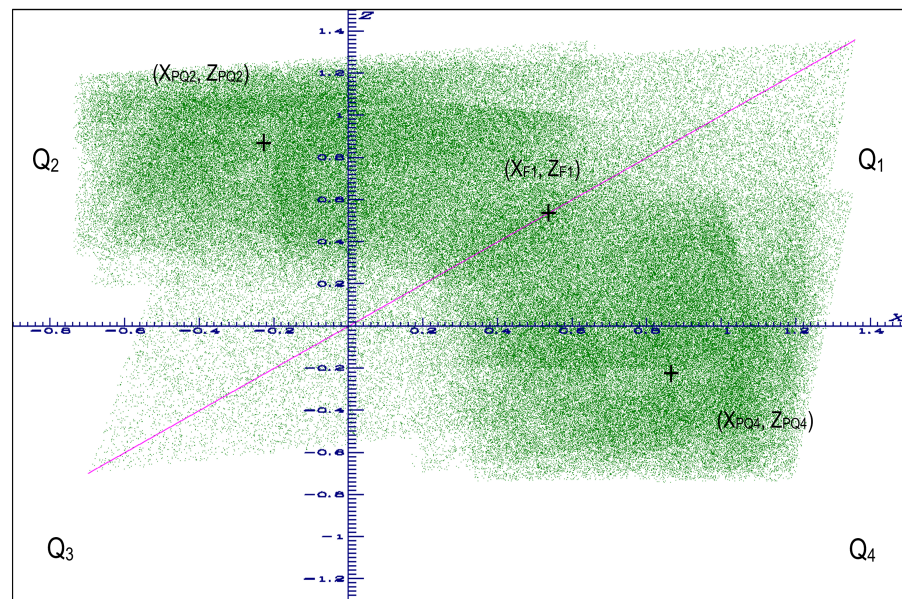


Figure 17. Projection onto the (x, z) -plane of the coexisting *sheet* and *thread* 3D Lozi map (35) hyperchaotic attractor for the parameter value $a = -1.25, b = 0.2, c = -1.25$. Initial value of the *thread*-attractor (in purple) $(x_0 = 0.125, y_0 = 0.2, z_0 = 0.125)$. Initial value of the *sheet*-attractor (green) $(x_0 = 0.1, y_0 = 0.2, z_0 = 0.1)$.

Hence, the dimension of the unstable invariant manifold of this fixed point is two (and that of the stable invariant manifold is one). However, in the plane $(x = z, y)$, the map (40) has only two eigenvalues:

$$\lambda_1 \approx -1.514171, \lambda_2 = +0.264171.$$

Therefore, in this plane, the unstable invariant manifold of this fixed point is only one-dimensional. This unstable invariant manifold is the skeleton of the *thread*-attractor. However, in Q_3 , there is no fixed point.

The other two fixed points (x_{F_2}, y_{F_2}) and (x_{F_4}, y_{F_4}) belong to Q_2 and Q_4 .

$$x_{F_2} = \frac{-2.65}{1.0625} \approx -2.49412, y_{F_2} = \frac{-0.4}{1.0625} \approx -0.376471, z_{F_2} = \frac{0.65}{1.0625} \approx 0.611765,$$

and

$$x_{F_4} = \frac{0.65}{1.0625} \approx 0.611765, y_{F_4} = \frac{-0.24}{1.0625} \approx -0.376471, z_{F_4} = \frac{-2.65}{1.0625} \approx -2.49412,$$

with, again, the symmetry

$$x_{F_2} = z_{F_4}, y_{F_2} = y_{F_4}, z_{F_2} = x_{F_4}.$$

There also exists a period-two orbit of the type discussed in the previous section:

$$x_{PQ_4} = \frac{212}{245} \approx 0.86531, y_{PQ_4} = \frac{32}{245} \approx 0.13061, z_{PQ_4} = \frac{-52}{245} \approx -0.21224;$$

$$x_{PQ_2} = z_{PQ_4}, y_{PQ_2} = y_{PQ_4}, z_{PQ_2} = x_{PQ_4}.$$

This case is similar to the first case; however, the two components of the *sheet* hyperchaotic attractor have merged (see Figures 16 and 17).

4.4.4. Case $a = -1.365$ and $a = -1.369$, $b = 0.36$, $c = 0.6$, Blow up of the Attractor versus the Parameter a

In this example, the rich dynamics of (36) are highlighted using an example where a very small change of 2‰ in the value of a leads to a blow up of the chaotic attractor (see Figures 18 and 19). When $a = -1.365$ (resp. $a = -1.369$), the Jacobian value is 0.27576 (resp. 0.27684).

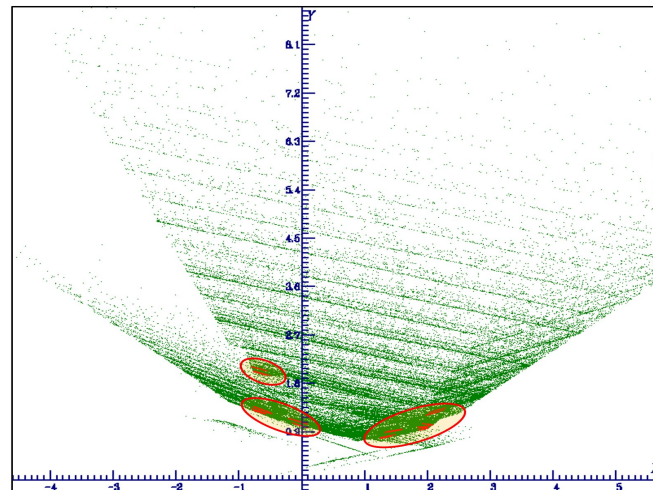


Figure 18. Projection onto the (x, y) -plane of two attractors of the 3D Lozi map (35) chaotic attractor for the parameter values $a = -1.365$ and $a = -1.369$, $b = 0.36$, $c = 0.6$. Initial value of both attractors ($x_0 = 0.2$, $y_0 = 0.1$, $z_0 = 0.0$). When $a = -1.365$, the attractor consists of small red lines (in the three oval regions surrounded by a red curve); instead, when $a = -1.369$, there is a blow up of the green attractor, which is partially displayed in this magnification of the (x, y) -phase plane.

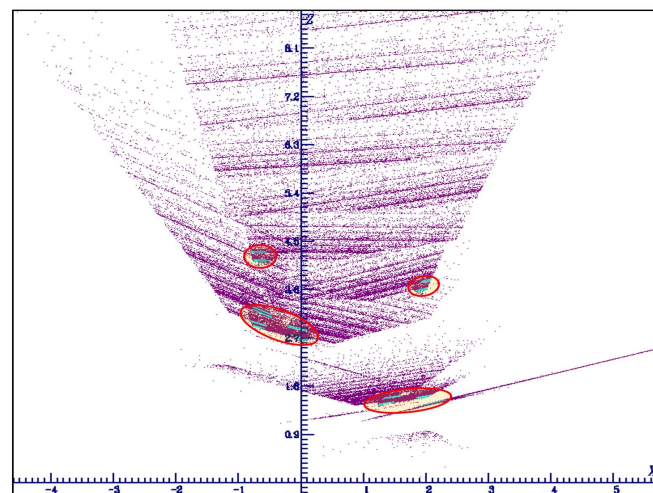


Figure 19. Projection onto the (x, z) -plane of two attractors of the 3D Lozi map (35) chaotic attractor for the parameter values $a = -1.365$ and $a = -1.369$, $b = 0.36$, $c = 0.6$. Initial value of both of the attractors ($x_0 = 0.2$, $y_0 = 0.1$, $z_0 = 0.0$). When $a = -1.365$, the attractor consists of small cyan lines (in the four oval regions surrounded by a red curve); instead, when $a = -1.369$, there is a blow up of the purple attractor, which is partially displayed in this magnification of the (x, z) -phase plane.

4.4.5. Case $a = -1.369$, $b = 0.02$ to $b = 0.36$, $c = 0.6$, Blow up of the Attractor versus the Parameter b

In this example, several values of the parameter b with the same value of $a = -1.369$ lead to a blowing up of the size of the chaotic attractor (see Figures 20 and 21). When

$b = 0.02$, the Jacobian value is 0.01538; for $b = 0.05$, the Jacobian value is 0.03845; for $b = 0.09$, the Jacobian value is 0.06921, and, for $b = 0.16$, the Jacobian value is 0.12304.

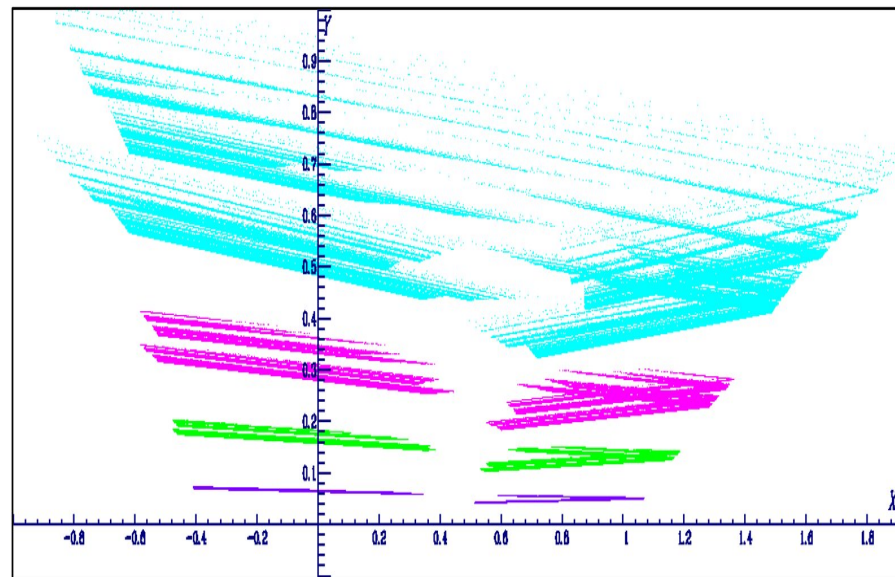


Figure 20. Projection onto the (x, y) -plane of two attractors of the 3D Lozi map (35) chaotic attractor for the parameter values $a = -1.369$, $c = 0.6$, $b = 0.02$ (purple), $b = 0.05$ (green), $b = 0.09$ (magenta), and $b = 0.16$ (cyan). Initial value for all attractors ($x_0 = 0.2$, $y_0 = 0.1$, $z_0 = 0.0$). The attractors for each value of b remain in a small bounded region of the (x, y) -plane. When b is increased (see next figure), there is a blowing up of the size of the attractor, which however remains bounded.

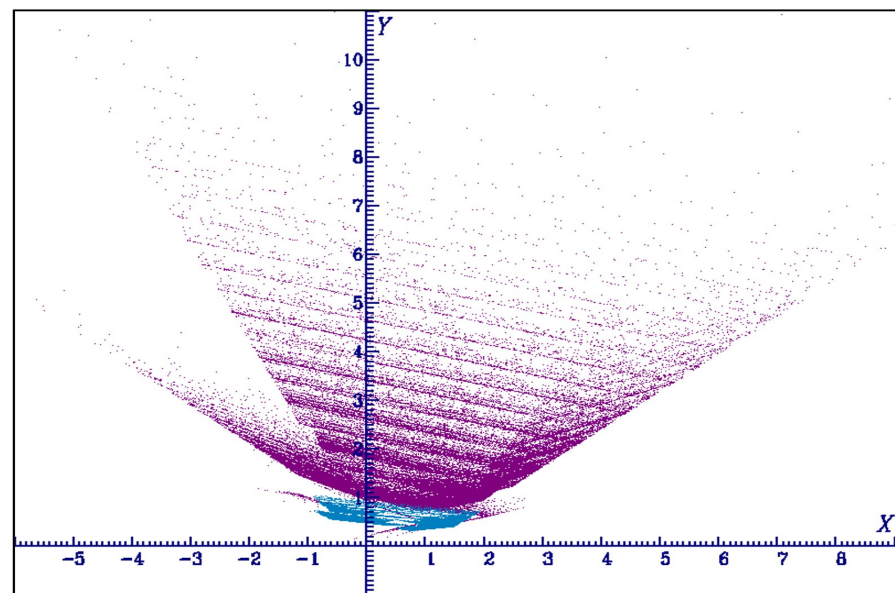


Figure 21. Continuation of the previous figure. Projection onto the (x, y) -plane of two attractors of the 3D Lozi map (35) chaotic attractor for the parameter values $a = -1.369$, $c = 0.6$, $b = 0.16$, (cyan), and $b = 0.36$ (purple). Initial value of both attractors ($x_0 = 0.2$, $y_0 = 0.1$, $z_0 = 0.0$). When $b = 0.16$, the attractor has a small size; instead, when $a = 0.36$, there is a blow up of the purple attractor, which is partially displayed in this magnification of the (x, y) -phase plane.

5. Conclusions

In this article, a three-dimensional piece-wise linear extension of the two-dimensional Lozi map was introduced that respects the constraint of a constant Jacobian. It displays a special property never highlighted before for chaotic mappings: the coexistence of *thread* chaotic attractors (i.e., attractors that are formed by a collection of lines) and *sheet* hyperchaotic attractors (i.e., attractors that are formed by collection of planes). This new three-dimensional mapping can generate a large variety of chaotic and hyperchaotic attractors. Five prototypical examples of such behavior were given. In the first three examples, there is the coexistence of *thread* and *sheet* chaotic attractors. However, their shapes are different and they are constituted by a different number of pieces. In the last two examples, the blow up of the attractors with respect to parameter a and b is highlighted.

Funding: This research received no external funding.

Institutional Review Board Statement: Not applicable.

Informed Consent Statement: Not applicable.

Data Availability Statement: Not applicable.

Acknowledgments: The author sincerely dedicates this manuscript to Michal Misiurewicz who first studied the two-dimensional map, proved the existence of a strange attractor and coined the name Lozi map.

Conflicts of Interest: The author declares no conflict of interest.

References

- Zeraoulia, E. *Lozi Mappings—Theory and Applications*; CRC Press: Boca Raton, FL, USA; London, UK; New York, NY, USA, 2013; 309p.
- Letellier, C.; Abraham, R.; Shepelyansky, D.L.; Rössler, O.E.; Holmes, P.; Lozi, R.; Glass, L.; Pikovsky, A.; Olsen, L.F.; Tsuda, I.; et al. Some elements for a history of the dynamical systems theory. *Chaos* **2021**, *31*, 053110. [CrossRef] [PubMed]
- Ruelle, D. Dynamical systems with turbulent behavior. In *Mathematical Problems in Theoretical Physics, Lecture Notes in Physics*; Dell’Antonio, G., Doplicher, S., Jona-Lasinio, G., Eds.; Springer: Berlin/Heidelberg, Germany, 1978; Volume 80, pp. 341–360; International Mathematics Physics Conference, Roma, 1977. [CrossRef]
- Lorenz, E.N. Deterministic nonperiodic flow. *J. Atmos. Sci.* **1963**, *20*, 130–141. [CrossRef]
- Hénon, M. A two-dimensional mapping with a strange attractor. *Commun. Math. Phys.* **1976**, *50*, 69–77. [CrossRef]
- Smale, S. Differentiable dynamical systems. I Diffeomorphisms. *Bull. Am. Math. Soc.* **1967**, *73*, 747–817. [CrossRef]
- Lozi, R. Un attracteur étrange (?) du type attracteur de Hénon. *J. Phys.* **1978**, *39*, C5–9–C5–10. [CrossRef]
- Misiurewicz, M. Strange attractors for the Lozi mappings. *Ann. N. Y. Acad. Sci.* **1980**, *357*, 348–358. [CrossRef]
- Misiurewicz, M.; Stimać, S. Symbolic dynamics for Lozi maps. *Nonlinearity* **2016**, *29*, 3031–3046. [CrossRef]
- Kucharski, P. Strange attractors for the family of orientation preserving Lozi Maps. *arXiv* **2022**, arXiv:2211.10296v1.
- Baptista, D.; Severino, R.; Vinagre, S. The basin of attraction of Lozi Mappings. *Int. J. Bifurc. Chaos* **2009**, *19*, 1043–1049. [CrossRef]
- Ishii, Y. Towards a kneading theory for Lozi mappings I: A solution of the pruning front conjecture and the first tangency problem. *Nonlinearity* **1997**, *10*, 731–747. [CrossRef]
- Boroński, J.P.; Kucharski, P.; Ou, D.-S. Lozi Maps with Periodic Points of All Periods $n > 13$. 2022. Available online: https://www.researchgate.net/publication/366740872_Lozi_maps_with_periodic_points_of_all_periods_n_13 (accessed on 27 April 2023).
- Botella-Soler, V.; Castelo, J. M.; Oteo, J. A.; Ros, J. Bifurcations in the Lozi map. *J. Phys. A Math. Theor.* **2011**, *44*, 305101. [CrossRef]
- Sushko, I.; Avrutin, V.; Gardini, L. Center Bifurcation in the Lozi Map. *Int. J. Bifurc. Chaos* **2021**, *31*, 2130046. [CrossRef]
- Glendinning, P.A.; Simpson, D.J.W. Chaos in the border-collision normal form: A computer-assisted proof using induced maps and invariant expanding cones. *Appl. Math. Comput.* **2022**, *434*, 127357. [CrossRef]
- Collet, P.; Levy, Y. Ergodic properties of the Lozi mappings. *Commun. Math. Phys.* **1984**, *93*, 461–482. [CrossRef]
- Rychlik, M. Invariant Measures and the Variational Principle for Lozi Mappings. In *The Theory of Chaotic Attractors*; Hunt, B.R., Li, T.Y., Kennedy, J.A., Nusse, H.E., Eds.; Springer: New York, NY, USA, 2004; [CrossRef]
- Cao, Y.; Liu, Z. The Geometric Structure of Strange Attractors in the Lozi Map. *Commun. Nonlinear Sci. Numer. Simul.* **1998**, *3*, 119–123. [CrossRef]
- Afraimovich, V.S.; Chernov, N.I.; Sataev, E.A. Statistical properties of 2-D generalized hyperbolic attractors. *Chaos* **1995**, *5*, 238–252.10.1063/1.166073. [CrossRef]
- Zheng, W.-M. Symbolic Dynamics for the Lozi Map. *Chaos Solitons Fractals* **1991**, *1*, 243–248. [CrossRef]

22. Ishii, Y. Towards a kneading theory for Lozi mappings II: Monotonicity of the Topological Entropy and Hausdorff Dimension of Attractors. *Commun. Math. Phys.* **1997**, *190*, 375–394. [CrossRef]
23. Ishii, Y.; Sands, D. Monotonicity of the Lozi family near the tent-maps. *Comm. Math. Phys.* **1998**, *198*, 397–406. [CrossRef]
24. de Carvalho, A.; Hall, T. How to prune a horseshoe. *Nonlinearity* **2002**, *15*, R19–R68. [CrossRef]
25. Li, H.; Li, K.; Chen, M.; Bao, B. Coexisting Infinite Orbits in an Area-Preserving Lozi Map. *Entropy* **2020**, *22*, 1119. [CrossRef] [PubMed]
26. Natiq, H.; Banerjee, S.; Ariffin, M.R.K.; Said, M.R.M. Can hyperchaotic maps with high complexity produce multistability? *Chaos* **2019**, *29*, 011103. [CrossRef]
27. Zhusubaliyev, Z.T.; Mosekilde, E. Multistability and hidden attractors in a multilevel DC/DC converter. *Math. Comput. Simul.* **2015**, *109*, 32–45. [CrossRef]
28. Bao, B.C.; Li, H.Z.; Zhu, L.; Zhang, X.; Chen, M. Initial-switched boosting bifurcations in 2D hyperchaotic map. *Chaos* **2020**, *30*, 033107. [CrossRef]
29. Zhang, L.-P.; Liu, Y.; Wei, Z.-C.; Jiang, H.-B.; Bi, Q.-S. A novel class of two-dimensional chaotic maps with infinitely many coexisting attractors. *Chin. Phys. B* **2020**, *29*, 060501. [CrossRef]
30. Bao, H.; Hua, Z.Y.; Wang, N.; Zhu, L.; Chen, M.; Bao, B.C. Initials-boosted coexisting chaos in a 2D Sine map and its hardware implementation. *IEEE Trans. Ind. Inform.* **2021**, *17*, 1132–1140. [CrossRef]
31. Lopesino, C.; Balibrea, F.; Wiggins, S.R.; Mancho, A.M. The Chaotic Saddle in the Lozi Map, Autonomous and Nonautonomous Versions. *Int. J. Bifurc. Chaos* **2015**, *25*, 1550184. [CrossRef]
32. Richter, H. The generalized Henon maps: Examples for higher-dimensional chaos. *Int. J. Bifurc. Chaos* **2002**, *12*, 1371–1384. [CrossRef]
33. Young, L.-S. A Bowen-Ruelle measure for certain piecewise hyperbolic maps. *Trans. Am. Math. Soc.* **1985**, *287*, 41–48. [CrossRef]
34. Misiurewicz, M.; Stimac, S. Lozi-like maps. *Discret. Contin. Dyn. Syst.* **2018**, *38*, 2965–2985. [CrossRef]
35. Juang, J.; Chang, Y.-C. Boundary influence on the entropy of a Lozi-type map. *J. Math. Anal. Appl.* **2010**, *371*, 728–740. [CrossRef]
36. Sakurai, A. Orbit shifted shadowing property of generalized Lozi map. *Taiwan. J. Math.* **2010**, *14*, 1609–1621. Available online: <https://www.jstor.org/stable/43834956> (accessed on 4 May 2023). [CrossRef]
37. Boronski, J.; Stimac, S. Densely branching trees as models for Hénon-like and Lozi-like attractors. *arXiv* **2022**, arXiv:2104.14780v2.
38. Kucharski, P. Strange attractors and densely branching trees for the generalized Lozi-like family. *arXiv* **2023**, arXiv:2302.04641.
39. Aiewcharoen, B.; Boonklurb, R.; Konglwan, N. Global and Local Behavior of the System of Piecewise Linear Difference Equations $x_{n+1} = |x_n| - y_n - b$ and $y_{n+1} = x_n - |y_n| + 1$ Where $b \geq 4$. *Mathematics* **2021**, *9*, 1390. [CrossRef]
40. Mammeri, M.; Kina, N. E. Dynamical properties of solutions in a 3-D Lozi map. In Proceedings of the 6th International Arab Conference on Mathematics and Computations (IACMC2019), Zarqa University, Zarqa, Jordan, 24–26 April 2019; pp. 27–33.
41. Joshi, Y.; Blackmore, D.; Rahman, A. Generalized Attracting Horseshoes and Chaotic Strange Attractors. *arXiv* **2020**, arXiv:1611.04133v2.
42. Bilal, S.; Ramaswamy, R. A higher-dimensional generalization of the Lozi map: Bifurcations and dynamics. *J. Differ. Equations Appl.* **2022**, *1–12*. [CrossRef]
43. Lozi, R. Strange attractors: A class of mapping of R^2 which leaves some Cantor sets invariant. In *Intrinsic Stochasticity in Plasmas*; Laval, G., Gresillon, D., Eds.; Les Editions de Physique; Orsay: Cargese, France, 1979; pp. 373–381.
44. Chutani, M.; Rao, N.; Nirmal Thyagu, N.; Gupte, N. Characterizing the complexity of time series networks of dynamical systems: A simplicial approach. *Chaos* **2020**, *30*, 013109. [CrossRef]
45. Khennaoui, A.-A.; Ouannas, A.; Bendoukha, S.; Grassi, G.; Lozi, R.; Pham, V.-T. On fractional-order discrete-time systems: Chaos, stabilization and synchronization. *Chaos Solitons Fractals* **2019**, *119*, 150–162. [CrossRef]
46. Ibrahim, R.W.; Baleanu, D. Global stability of local fractional Hénon-Lozi map using fixed point theory. *AIMS Math.* **2022**, *7*, 11399–11416. [CrossRef]
47. Aliwi, B.H.; Ajeena, R.K.K. A performed knapsack problem on the fuzzy chaos cryptosystem with cosine Lozi chaotic map. *AIP Conf. Proc.* **2023**, *2414*, 040047. [CrossRef]
48. Aliwi, B.H.; Ajeena, R.K.K. On Fuzzy Sine Chaotic Based Model in Security Communications. *J. Posit. Sch. Psychol.* **2022**, *6*, 8127–8133. Available online: <https://journalppw.com/index.php/jjpsp/article/view/5169> (accessed on 4 May 2023).
49. Cano, A.V.; Cosenza, M.G. Chimeras and clusters in networks of hyperbolic chaotic oscillators. *Phys. Rev. E* **2017**, *95*, 030202(R). [CrossRef] [PubMed]
50. Semenova, N.; Vadivasova, T.; Anishchenko, V. Mechanism of solitary state appearance in an ensemble of nonlocally coupled Lozi maps. *Eur. Phys. J. Spec. Top.* **2018**, *227*, 1173–1183. [CrossRef]
51. Anishchenko, V.; Rybalova, E.; Semenova, N. Chimera States in two coupled ensembles of Henon and Lozi maps. Controlling chimera states. *AIP Conf. Proc.* **2018**, *1978*, 470013-1–470013-4. [CrossRef]
52. Rössler, O.E.; Hudson, J.L.; Farmer, J.D. Noodle-map chaos: A simple example. In *Stochastic Phenomena and Chaotic Behaviour in Complex Systems*; Schuster, P., Ed.; Springer Series in Synergetics; Springer: Berlin/Heidelberg, Germany, 1984; Volume 21. [CrossRef]
53. Rössler, O.E. An equation for hyperchaos. *Phys. Lett.* **1979**, *71A*, 155–157. [CrossRef]
54. Anosov, D.V. Dynamical Systems IX: Dynamical Systems with Hyperbolic Behaviour. In *Encyclopedia of Mathematical Sciences: Vol. 9*; Springer: Berlin/Heidelberg, Germany, 1995. [CrossRef]

55. Elhadj, Z.; Sprott, J.C. *Robust Chaos and Its Applications*; World Scientific Series on Nonlinear Science Series A; World Scientific: Singapore, 2011; Volume 79. [CrossRef]
56. Kuznetsov, S. P. Some lattice models with hyperbolic chaotic attractors. *Russ. J. Nonlinear Dyn.* **2020**, *16*, 13–21. [CrossRef]
57. Kilassa Kvaternik, K. Tangential Homoclinic Points Locus of the Lozi Maps. Doctoral Thesis, University of Zagreb, Zagreb, Croatia, 2022; 110p. Available online: <https://repozitorij.pmf.unizg.hr/islandora/object/pmf:11546> (accessed on 27 April 2023).

Disclaimer/Publisher's Note: The statements, opinions and data contained in all publications are solely those of the individual author(s) and contributor(s) and not of MDPI and/or the editor(s). MDPI and/or the editor(s) disclaim responsibility for any injury to people or property resulting from any ideas, methods, instructions or products referred to in the content.